EVALUATION OF THERMAL PROPERTIES AND AIR VOID

CHARACTERISTICS OF POROUS CONCRETE

BY

PENGYU XIE

A thesis submitted to the

School of Graduate Studies

Rutgers, The State University of New Jersey

In partial fulfilment of the requirements

For the degree of

Master of Science

Graduate Program in Civil and Environmental

Engineering

Written under the Direction of

Hao Wang

And approved by

New Brunswick, New Jersey

[OCTOBER 2017]

ABSTRACT OF THE THESIS

Evaluation of Thermal Properties and Air Void Characteristics of Porous Concrete

by Pengyu Xie

Thesis Director:

Hao Wang

Porous concrete is becoming an attractive pavement solution due to its great performances in mitigating urban heat island (UHI) effect and managing storm water. As a heterogeneous material, the properties of cement-based porous concrete are complicated to quantify and hard to predict. This thesis focused on the evaluation of thermal properties and air void characteristics of porous concrete.

The thermal properties of aggregates, cement pastes, and porous concretes were measured by transient plate method (TPS) and steady-state heat flow meter method, respectively. X-ray computed tomography (CT) technique was utilized and three-dimensional (3-D) pictures were treated to analyze the microscopic structure of air voids in porous concrete. The existing analytical models were employed to estimate thermal conductivity of pervious concretes and compared to experimental measurements.

The tests results show that thermal conductivity and heat capacity of cement paste increases as water cement ratio increases. Meanwhile, for the same mix design, the thermal properties of different cement paste samples had few variations. However, the porous concrete is very heterogeneous and the same mix design cannot ensure the similar porosity; instead, significant variations of porosity were observed.

The existing analytical results did not show satisfactory prediction results of thermal conductivity as compared to testing results. This indicates the existing models are not suitable to estimate the thermal conductivity of porous concrete. This is because the models ignore the complex microscopic structures of porous concrete.

Based on the CT-scanned images, within the horizontal plane of cylindrical sample, slight differences of normalized projected lengths of air voids were observed in the orthogonal horizontal directions; while the normalized projected length of connected voids in vertical direction was found smaller than those in horizontal directions. The smaller aggregates tend to form the longer air void length in porous concrete. The curvatures of air voids for smaller aggregates are greater than that of larger aggregates. Meanwhile, within the same mix design, the curvature of air voids increases with the increasing of porosity. The porosity and aggregate size do not have significant influences on the ellipticity and tortuosity of air voids within porous concrete. However, with the increase of porosity, the air voids tend to have the greater equivalent diameter.

ACKNOWLEDGEMENT

Foremost, I would like to express my sincere gratitude to my advisor Dr. Hao Wang for the continuous support of my Master's study and research, for his patience, motivation, enthusiasm, and immense knowledge. His guidance helped me in all the time of research and writing of this thesis and it has been a pleasure working with him.

Besides my advisor, I would like to thank the rest of my thesis committee: Dr. Najm and Dr. Nassif, for their encouragement, insightful comments, and hard questions.

I thank my fellow friends in our research group: Jun Chen, Jiaqi Chen, Wei Sun and Xiaodan Chen. Their friendship helped me through the hard times during these two years. I thank Dr. Jun Chen especially here for the help he offered me and the discussions we had together.

Finally, I would like to thank my parents, Yaogang Xie and Jianying Pei, my cousin Xin Xie and Ran Xie for all of their love, guidance, and their persistent trust in me.

TABLE OF CONTENT

CHAPTER 1. INTRODUCTION

1.1 Background

Transportation infrastructure is vitally important for human beings. Highway transportation, as an important component of transportation system, is irreplaceable because of its flexibility and adaptability. Cargos or travelers are able to be directly transported from originations to destinations without any transfer or hiatus, achieving "door-to-door" solutions. Meanwhile, highway infrastructure is also easy to be constructed and maintained with relatively fewer investments. Pavement, which is defined as the layered structure placed on existing foundation, plays a crucial role in highway infrastructure. Well-designed pavement should not only provide comfortable driving, but also ensure the safety of road users.

Nowadays, three main categories of pavements, flexible, rigid, and composite, are extensively used in highway through the whole world. Flexible pavements are those with asphalt concrete as surface layer, while rigid pavements have Poland cement concrete (PCC) on the surface. Composite pavements are the pavement having both asphalt concrete layer and PCC layer.

Due to the differences in material properties, flexible and rigid pavements have their own advantages and disadvantages. Compared with rigid pavements, flexible ones have better serviceability and lower tire-pavement noise. Besides, flexible pavements are easy for maintenance and can be recycled for further pavement construction. On the other side, rigid pavements have considerable advantages in carrying heavy traffic loading and better durability *(Susana and Ferreira 2014; Krishnamoorthy et al. 2016; Mamlouk and Zaniewski 1998.; Lee 2017; Tsai et al. 2010).*

Although flexible pavements have been widely used, they may cause negative impacts on environment. In the well-developed urban areas, pavement system not only replaces vegetation and soil with an impermeable surface, but also increase the temperature of adjacent areas due to it high solar adsorption *(Li et al. 2013).* Thus, environment-friendly pavement solutions should be studied.

Porous concrete is a particular kind of concrete, which is also called as pervious concrete or permeable concrete, with a high volume of connected voids so that water on pavement surface is able to directly permeate downward. Porous concrete consists of coarse aggregates and cement paste while having few filler. The skeleton structure of porous concrete is mainly made of coarse aggregates, which is covered by thin cement paste film to adhere aggregates together. The lack of fine aggregates induces a large proportion of connected voids and better porosity, ranging from 15% to 30%. *(Niyazuddin and Selvan 2017)*

To some extent, the mechanical strength of porous concretes is lower than that of conventional ones. Hence, porous concrete is traditionally used in light traffic areas like road shoulders, parking lots, and residential streets.

The large volume of continuous pores in porous concrete facilitates the infiltration of storm water which reduces surface run-off in urban areas and provides groundwater supplementation and recharge *(Zhang et al. 2015).* Meanwhile, the interconnected pores offer the channels for water to evaporate and escape, with a phase change process absorbing heat and reducing the temperature of pavements *(Li et al. 2013)*. What's more, porous concrete also have a good performance in tire-pavement noise reduction, which is good for noise reduction and save enormous cost on building and maintaining of noise barriers *(Tian et al. 2014)*.

Compared to conventional pavements, porous concrete pavements have better performance in mitigating urban heat island (UHI) effect. For asphalt pavements, their black surfaces absorb much more heat than concrete ones, leading to a higher surface temperature. In addition, porous concrete pavement stores less heat than conventional concrete pavements, helping reducing heat island effect in urban areas *(Santamouris 2013)*. Whereas, some researchers reported that the surface temperatures of porous concrete pavements are higher than those of conventional ones *(Zhang 2015; Qin 2015)*. One possible explanation for this phenomenon is that the large-area connected air void impact the thermal conductivity of porous concrete.

1.2 Problem Statement

With the population increase and urban expansion, environmental friendliness and sustainability become more and more important. Porous concrete has been studied in many researches to evaluate how the porous structures affect its mechanical and hydraulic properties. However, the thermal properties of porous concrete are vital since the effect of porous concrete can be directly influenced about pavement surface temperature and ambient temperature. Previous researches have shown that the void characteristics significantly affect thermal properties of composite materials *(Khan*

2002; Chen et al. 2015). Thus, microscopic void structure model is necessary to resolve how thermal properties are influenced by air voids.

In addition, analytical methods were proposed to estimate the effective thermal conductivity of compound material based on its composition and components' properties *(Wang et al. 2006)*. However, the applicability of these models on porous concrete has not been studied. Limited researches have focused on the relationship between microscopic void characteristics and the effective thermal conductivity of porous concrete. If an accurate relationship could be established between void structures and the effective thermal conductivity of porous concrete, the appropriate mix composition and gradation can be selected for the targeted thermal properties.

1.3 Objective

The primary objective of this thesis is to evaluate microscopic air void structure and thermal properties of porous concrete. These results can be used for further understanding of thermal transport in porous media in general.

To achieve the objective, the following tasks were conducted

(1) Measure thermal conductivities of porous concretes, cement pastes, and coarse aggregates.

(2) Analyze CT-scanned images and conduct quantitative analysis on the characteristics of air voids in porous concretes.

(3) Predict the effective thermal properties of porous concrete by existing models then compare to experimental results.

1.4 Thesis Outline

The thesis report consists of five chapters. The first chapter presents the background of research, problem of statement, and objective. The second chapter is literature review, summarizing measurement methods, the factors influencing thermal conductivity of porous concrete, and the methods of analyzing air voids inside porous concrete. The third chapter presents tests results of thermal properties of porous concrete and its components. The fourth chapter presents analytical prediction of thermal properties and the analysis of microscopic void properties in porous concrete. The Fifth chapter summarizes the findings and future research recommendations.

CHAPTER 2. LITERATURE REVIEW

2.1 Experimental Methods to Measure Thermal Properties

Generally, two principles are involved in measuring thermal properties of bulk materials, steady state method and transient method. Based on these principles, several methods are developed to fit various samples and work conditions.

2.1.1 Steady State Method

Steady-state measurement needs the tested sample's temperature field reaching to a stabilized distribution, then calculates thermal conductivity by recording the heat flow Q and temperature difference ΔT at a specific distance *(Zhao et al. 2016)*. Guarded-hot plate, comparative and parallel thermal conductance technique are three commonly used steady-state measurements.

Traditional guarded-hot plate method is a standard technique for measuring bulk materials with high accuracy. However, this method is very rigid at the sample size and measurement temperature, which may not universal for all tests. Thus, some researchers modified the traditional guarded-hot plate method in order to achieve their purposes.

Kočí et al. (2012) measured the apparent thermal conductivity of large non-homogenous hollow clay bricks by the guarded hot plate experiment. Account for the fact that their sample is too big to fit into the traditional guarded-hot plate apparatus, a modified equipment is proposed. Numerical analysis was involved to correct the errors during measurement, including quantifying heat losses and modifying heat fluxes, which were given by heat losses due to the enlargement of the measurement chamber.

The iteration processes were conducted until the calculated and measured thermal transfer coefficients are the same. This process ensures the accuracy of the whole measurement.

Considering the traditional guarded hot plate method is limited to the temperature range from -20$^\circ C$ to 80$^\circ C$, *Scoarnec et al. (2014)* proposed a modified version to measure thermal conductivity of materials at high temperature. According to the principle of guarded hot plate method, the measurement temperature would not affect the thermal conductivity. The accuracy of modified apparatus is verified by conducting comparative measurements on rectified and typical reference material from 23$^\circ C$ to 600$^\circ C$, with relative deviations less than 5% over the whole thermal conductivities (up to 15 W/mK) and temperature ranges.

Apart from guarded hot plate method, the comparative technique like guarded heat flow meter method is also a very prevalent steady state method. *Yoon et al. (2014)* proposed a new analytic method to measure thermal properties based on the guarded heat flow meter device. Their tests can be separated into two sections. The first step was determining the thermal conductivity and contact resistance by meter's signal under steady states and linear regression analysis. Then the non-steady-state test and nonlinear regression analysis was employed to obtain thermal diffusivity and specific heat capacity of materials. Meanwhile, they suggested the proper sample thicknesses of 50-100 mm when conducting transient tests, suitable for cement pastes and similar materials.

Brütting et al. (2016) proposed a method to measure specific heat capacity of phase change materials by guarded heat flow apparatus. Instead of using steady-state heat flow, they carried out a transient temperature step at the top and bottom of the sample to determine apparent heat flux. The specific heat capacity was calculated from apparent heat flux with the knowledge of reference thermal properties. Meanwhile, they introduced a correction factor, which only related to the geometry of the experimental setup, to represent the portion of heat stored in the reference bars. Several numerical simulations were conducted to validate the accuracy of this method, which showed good agreement.

When the sample size reaches millimeter scale, it is very challenging to measure temperature and heat flux *(Zhao et al. 2016). Zawilski et al.(2001)* suggested a method that is called parallel thermal conductance (PTC) technique, to measure small needle-like samples, which with a small cross-section area with respect to overall sample length. Instead of measurement thermal conductivity directly, the PTC measured the thermal conductance and needed a precise cross-sectional area to calculate thermal conductivity. One drawback of this method is that the measurement of dimension is able to bring relatively large degree of uncertainty in calculating the thermal conductivity. *Dasgupta and Umarji (2007)* used this technique to measure the thermal conductivity of $MoSi_2$ with minor aluminum substitutions at room temperature. The results indicate that with the aluminum substitution, a desecration would be expected on thermal conductivity except in the biphasic region.

2.1.2 Transient Methods

Due to the parasitic heat losses, contact resistance of temperature sensors, and long waiting time of steady state method, transient measurement methods have been developed and become a preferable measuring method. Unlike steady-state measurement which requires constant heat resources, periodically or pulse-like heat resources are employed in transient measurement, generating periodic (phase signal output) or transient (amplitude signal output) temperature changes in the specimen. Three commonly used transient techniques, namely pulsed power technique, hot-wire method and transient plane source (TPS) method have been developed to precisely calculate thermal conductivity.

Hot-wire method is a commonly used transient technique which the thermal properties are acquired from temperature verse time response, account for a heat flux generated by a linear heat source embedded in the test sample. *Ukrainczyk and Matusinović (2010)* carried out the transient hot wire method corresponding to the numerical approach, to obtain thermal diffusivity and thermal conductivity of calcium aluminate cement during hydration. According to their research, thermal diffusivity would decrease and increase with hydration when it happened at 15 $^{\circ}C$ and 30 $^{\circ}C$, respectively. The thermal conductivity of material increased with the temperature varied from 20 $^{\circ}C$ to 80 $^{\circ}C$.

In order to eliminate the effect of contact resistance between hot wire and sample, *Assael et al. (2015)* proposed a novel hot wire instrument to measure the thermal conductivity of solids. Account for the cutting-edged software suite combined with new electronic circuit, taking advantage of the Bayesian Optimization, they reduced the measurement time by 5 minutes. Several reference materials like Pyroceram 9606 and Pyrex 7740 were employed to validate the method, gaining good results with absolute uncertainty of 2%.

Pulsed power technique uses periodic electrical current to heat samples. It was first introduced by *Maldonado (1992)* to reduce long waiting time for both temperature stabilization and forming stabilized thermal gradient. The sample was sandwiched between heater and cooler. By applying periodic current, a small temperature gradient was created between two ends of sample which can be measured by thermocouple. Thermal properties were calculated based on analytic method and validated by steady-state method. *Kennedy and White (2005)* applied the method to investigate the thermal properties of ZrW_2O_8, which was a negative thermal expansion material. The test results were validated by laser-flash thermal diffusivity method, showing that ZrW_2O_8 has a very low thermal conductivity, which is able to make thermoelectric cooling material.

TPS method stands for transient plane source method, utilizing a plane sensor sandwiched between two halves of sample to determine thermal conductivity, thermal diffusivity and specific heat capacity simultaneously from a single measurement. *Bouguerra et al. (2001)* implemented TPS tests on wood composites material to evaluate its thermal conductivity, thermal diffusivity and specific heat capacity. The test results indicate that TPS is able to measure the thermal properties of highly porous materials, instead of merely isotropic materials.

Bentz (2007) carried out TPS technique to measure thermal conductivity and specific heat capacity of hydrated cement pastes. The analytical method was employed to estimate specific heat capacity as a function of degree of hydration for two curing conditions. Considering the Hashin-Shtrikman bounds, the thermal conductivity of cement powder was also estimated based on the measured thermal conductivity of the fresh paste and known thermal conductivity of water.

2.2 Factors That Influence Thermal Properties of Porous Concrete

Since porous concrete consists of cement paste, aggregates and air void, each phase would affect the effective thermal properties of composite material. This section reviewed some literatures that focused on these components and their relationship with thermal properties of porous concrete.

2.2.1 Cement Paste

Cement paste is the mixture of cement powder and water, mixing with specific water-cement ratio. It is called mortar when the sand is added. To improve thermal or mechanical properties, some additives are usually mixed with paste or mortar. *Fu and Chung (1999)* studied the thermal behavior of cement pastes with additives of silica fume, later, methylcellulose and short carbon fibers. From his results, silica fume, latex and methylcellulose significantly decrease the thermal conductivity of cement pastes, due to the relatively low conductivity of these admixtures. The carbon fibers are failed to increase the thermal conductivity as expected because adding them also increased the void content of cement paste.

Kim et al. (2003) used QTM-D3 tester to investigate how water-cement ratio and types of admixtures influenced the effective thermal conductivity of concrete. According to the experimental results, thermal conductivity had apparently decreased as the increment of water-cement ratio. Meanwhile, the common additives slag and fly ash also had negative effects on the effective thermal conductivity of concrete. In the tests, moisture condition dramatically increased the test results, when the samples changed from dry condition to saturated condition. The author stated that this phenomenon was account for changes in air voids filled with water, whole thermal conductivity is higher than that of air.

Dehdezi et al. (2013) studied the influence of phase change materials (PCMs) on the thermal properties of concrete. Different amount of microencapsulated PCMs were added into concrete and thermal tests was conducted. Experimental results showed that with the increase of PCMs content, the thermal conductivity and thermal diffusivity decrease since the microencapsulated structure will increase the air void content in the concrete. Meanwhile, within the temperature period of PCM melting, the specific heat capacity of modified concrete increased significantly, which is capable of buffing of max/min temperature variations about the mean or delay of peak temperature occurrence.

Liu et al. (2015) added iron ore sand (IOS) into cement mortar to increase thermal conductivity for deicing and snow melting proposes. They use hot wire technique to determine the influence of water-cement ratio, total sand-cement ratio, river sand-iron ore sand ratio on the thermal conductivity of IOS mortar. Experimental results were analyzed by SPSS partial correlation and indicated that river sand-iron ore sand ratio had the best effect on thermal conductivity, followed by water-cement ratio, total sand-cement ratio in sequence.

Torres et al. (2015) comprehensively investigate the correlation of some important factors for porous concrete, including porosity, permeability, compressive and tensile strength versus thickness of cement paste. It was found that content of cement has an influence on the paste thickness and porosity of concrete. Expectably, the permeability and void space reduced with the increase of paste thickness. In addition, 28D compressive and tensile strength increased with paste thickness.

2.2.2 Aggregates

Since aggregates constitute the framework and main heat flux channel within porous concrete, it is very valuable to explore the thermal properties of aggregate. *Khan (2002)* evaluated the influence of different types of aggregates on thermal conductivity of concrete. Four types of rock were utilized as aggregate within concretes, limestone, siltstone, basalt and quartzite, ranked from lowest to highest thermal conductivity. The test results indicated that the thermal conductivities of concretes had proportion relationship with corresponding aggregates. Besides, Campbell-Allen and Thorne's model were employed to predict the influence of aggregate type on thermal conductivity of concrete. He stated that when the aggregate had low conductivity, the model had good agreement with measurement results.

Wang et al. (2015) prepared a new type of foam concrete, which using clay ceramsite as aggregate, to evaluate the thermal properties variation with ceramsite volume proportion. Results showed that thermal conductivity had a positive correlation with dry density and compressive strength of concrete. They also proposed a polynomial model to estimate thermal conductivity of ceramsite cellular concrete by its dry density and compressive.

Fenollera et al. (2015) laid their focus on the thermal properties of recycled aggregate for the purpose of improving concrete performance. Experiments were performed on the self-compacting concrete with different recycled aggregate doped. Thermal conductivity were quantified at three temperatures 20℃, 25℃ and 30℃ with infrared thermography and heat flow meter. By comparing the experimental results, conclusions can be drawn that thermal conductivity decreases with temperature and RA percentage. However, two different thermal behaviors are put forward for self-compacting concrete with different RA fraction.

2.2.3 Air Void

For porous concrete, air void has primary impacts on its properties, not matter in mechanical, thermal or hydraulic. *Miled and Limam (2016)* derived five well-known Mean Field Homogenization schemes to predict thermal conductivities of foam concretes, the Voigt model, the Dilute method, the Mori-Tanaka model, the Self

Consistent model and the Differential method. The only independent variable for each model is porosity. They found that the predicted thermal conductivities were very close when the porosity is small, while for the concrete with large air void content, the predictions were very difference. Thus, a homogenization scheme was proposed by comparing analytic results with FEM simulation results.

Batool and Bindiganavile (2017) studied how air void size distribution influenced the thermal conductivity of foam concrete. By adding admixture into concrete, they concluded that fly ash and metakaolin would increase the porosity, which silica fume would reduce the porosity. When the median diameter value increased, the thermal conductivity would reduce, while smaller pores had crucial influence on thermal conductivity.

2.3 Pore Characteristic of Porous Concrete

Aboufoul et al. (2016) comprehensively analyzed several tomographic properties of air voids in asphalt mixture, including air void content, average void diameter, Euler number, genus, enclosed cavities, etc. The results showed that with the increase of air void content, average void diameter increases while Euler number, enclosed cavities and tortuosity decreases. Furthermore, air void content also has impact on air voids perimeter, aspect ratio, circularity and roundness. In addition, through quantitative analyses of X-ray scanned results, a hydraulic conductivity model for asphalt mixture was established based on both statistical and physical concern, and it was proved to achieve a supreme predictive ability.

Promentilla et al. (2016) utilized three-dimensional image analysis techniques to study the impact of pore size, porosity, tortuosity and permeability on properties of concrete. Numerical simulation were conducted based on 3D image extraction. Regarding all the tested samples, effective porosity, pore size, geometric tortuosity and water permeability are demonstrated within a certain range respectively. Moreover, results also showed these parameters has specific relations, for example, geometric tortuosity increases with effective porosity, while permeability decreases in the contrary.

Wong et al. (2012) proposed a novel topological method to evaluate the cementitious materials' permeability. The pore structure was ideally regarded as a cubic lattice firstly, then a hydraulic radius approximation was employed to estimate the hydraulic conductance. At last Kirkpatrick's effective medium equation was utilized for obtaining effective pores conductance and further derive the macroscopic permeability. By comparison of the estimated value of this method and results from experimental tests, it was found out that the predicted values are significantly close to tested ones, which means the model has comparable accuracy to describe the permeability of cement materials.

Zhang et al. (2012) attempted to quantify the relation between mass diffusivity and X-rayed microstructure three-dimensional image for cement-based materials. A number of X-ray imaged are generated by scanning the cement paste samples with W/C ratio 0.50 at curing ages of 1,3,7,28 and 120 days, and then the 3D pore microstructure was obtained through topological analyses. Then the pore connectivity and permeability of each specimen are analyzed by cluster-labeling algorithm and finite element methods.

The results shows that the simulated diffusivity was generally consistent with the experimental investigation, which validates X-ray a reliable non-destructive technique tool to predict the permeability properties of cement-based materials.

CHAPTER 3. MEASUREMENT OF THERMAL PROPERTIES OF POROUS CONCRETE AND ITS COMPONENTS

This chapter summarizes the specific procedures of thermal experiments, which were employed to investigate thermal conductivity of porous concrete. Two thermal tests, TPS test and heat flow meter test, were mainly carried out.

3.1 Specimen Preparation

The main cementitious material used in the test is the ASTM type I ordinary Portland cement from Sakrete company, whose physical and chemical properties meet the requirements of ASTM C150. The aggregates with two different particle sizes are from the local quarry in New Jersey. The three mix designs of porous concrete are listed in Table 3.1. Figure 3-1 showed the pictures of porous concrete.

Table 3.1 Mix Proportion of Porous Concrete (lbs / yd^3)

Mix	Cement	3/8 aggregates	1/4 aggregates	Fly ash	Water	MRWR (SP)	HS	AE	Porosity
PRC-3	600	2835	--	--	162	1.9	1.9	0.8	24.30%
PRC-7	525	2500	--	95	168	1.9	1.9	0.8	26.33%
PRC-9	500	--	2700	--	165	--	--	0.8	24.92%

MRWR: Mid-Range Water Reducers HS: High Strength (Water Reducers)

AE: Air Entrainer

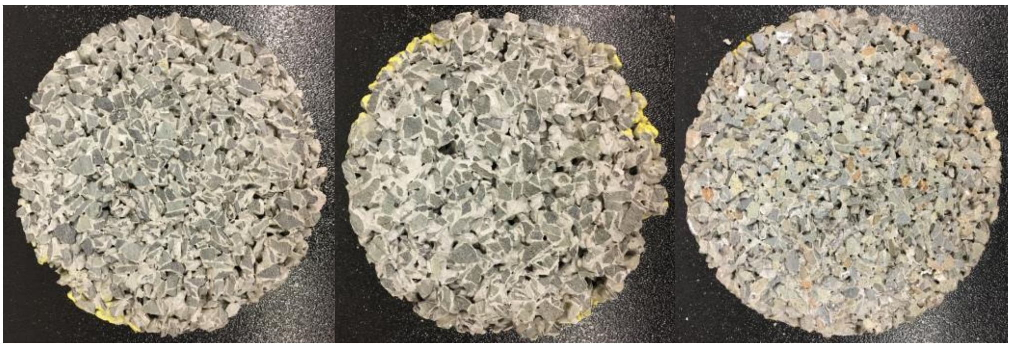

(a) (b) (c)

Figure 3-1 Porous concrete samples: (a) PRC-3; (b) PRC-7; and (c) PRC-9

Several cylindrical porous concrete samples and cylindrical cement paste samples were prepared for thermal tests. The dimension of concrete and cement paste samples were 6’’ by 12’’ and 3’’ by 6’’, respectively. The cement pastes had the same mix proportion with corresponding porous concrete, except the exclusion of aggregates. After being curried for 28 days, both heads of each cylindrical sample were chopped off and then were cut up into thin layers to fit into test apparatus. This process avoids uneven surface which will influence the measurement precision, especially for TPS method.

The air void contents of porous concrete were measured based on the method introduced by *Crouch et al.* (2003), which could be calculated by Equation (1):

$$\text{Air void content} = (1-\frac{G_{mb}}{G_{mm}})\times 100\% \qquad (1)$$

Where,

G_{mb} is the bulk specific gravity of porous concrete;

G_{mm} is the theoretical maximum specific gravity of porous concrete.

The bulk specific gravity and the theoretical maximum specific gravity of porous concrete can be calculated by Equation (2) and (3):

$$G_{mb} = \frac{A}{B - C - (B - A)/F} \tag{2}$$

$$G_{mm} = \frac{A}{A - D} \tag{3}$$

Where,

A is the mass of dry sample

B is the mass of sealed dry sample

C is the mass of sealed submerged sample

D is the mass of submerged sample

F is the apparent specific gravity of the sealing bag at 25°C, which is provided by the manufacturer.

The basic procedures of test are described below:

(1) Determine the mass of dry sample A and the mass of sealed vacuumed sample with plastic bag B

(2) Determine the submerged mass of sealed sample C.

(3) Cut the bag to allow water to enter the bag. Determine the mass of submerged, water-saturated sample D.

(4) Calculate air void content by Equation (1), (2) and (3).

All thermal tests were conducted at 20°C and dry condition. Aggregates rocks were also cut into thin layers to measure thermal properties. The dimension and measurement method of samples were listed in Table 3.2.

Table 3.2 Sample Preparation and Test

	No. of Samples	Diameter	Height	Thermal Measurement Method
Porous Concrete	18	152mm (6")	25mm (0.98")	Heat Flow Method
Cement Paste	9	76 m (3")	38mm (1.5")	Transient Plane Source (TPS) Method
Aggregate	10	38mm (2") Cubic	38mm (1.5")	Transient Plane Source (TPS) Method

3.2 Transient Plane Source Method

3.2.1 Test Equipment

The Transient Plane Source (TPS) method is generally used to measure thermal properties account for its convenience and accuracy. The Hot Disk TPS 500 Thermal Constants Analyzer was utilized in the research. TPS 500 system consisted of hardware part and software part. The tests were conducted by hardware part while the measured data were stored and calculated by software installed in a computer. The TPS 500 apparatus was illustrated in Figure 3-2.

Figure 3-2 TPS apparatus

The sensor is one of the most crucial components for TPS system, which has an electrically conducting pattern in the shape of a double spiral etched out of a thin sheet of nickel. This conducting pattern is covered by two thin sheets of insulating material, either Kapton or Mica, thickening the total thickness of sensor between 60 and 80 μm. The temperature ranges of measurement are up to 300ºC for Kapton layer and 1000ºC for Mica layers, respectively. The sensor would be sandwiched between two samples and run constant current when performing a test. This current would be strong enough to heat the sensor, making the sensor work as both heater and temperature detector. By recording the temperature change with time, the thermal properties of samples were measured and calculated by TPS 500 software. (*Thermtest Inc., 2015*)

3.2.2 Measurement Principles

The sensor would be heated when current pass through, with the resistance of sensor increased as a function of time, as shown in the following equation:

$$R(t) = R_0 \left\{1 + \alpha \cdot \left[\Delta T_i + \Delta T_{ave}(\tau)\right]\right\} \tag{4}$$

Where,

R_0 is the resistance of the sensor before heating;

α is the temperature coefficient of the resistivity;

ΔT_i is the constant temperature difference at two sides of sensor layers to indicate the thermal contact between sensor and sample surface, with $\Delta T_i = 0$ representing a perfect thermal contact;

$T_{ave}(\tau)$ is the temperature increase of the sample surface facing the sensor.

In Figure 3-3, the blue curve and red curve illustrate the temperature increase of sensor and sample surface during the measurement period, respectively. A constant difference ΔT_i can be observed after the short period of time Δt_i . (*Thermtest Inc., 2015*)

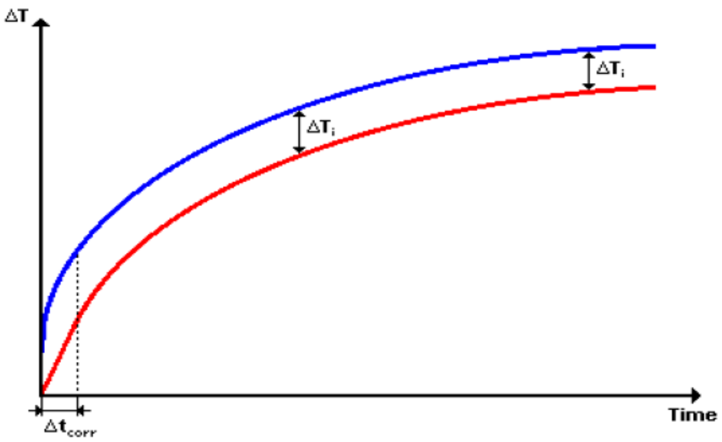

Figure 3-3 Temperature increasing curves of sensor and sample (*Thermtest Inc., 2015*)

From Equation (4) above, it's easy to get the temperature increase record by sensor, as shown in Equation (5):

$$\Delta T_i + \Delta T_{ave}(\tau) = \frac{1}{\alpha} \cdot \left(\frac{R(t)}{R_0} - 1 \right) \tag{5}$$

ΔT_i is constant during a very short period of time Δt_i, which could be calculated by Equation (6):

$$\Delta t_i = \frac{\delta^2}{\kappa_i} \tag{6}$$

Where,

δ is the thickness of insulating layer; and

κ_i is the thermal diffusivity of the insulating layer material.

The temperature increase of samples is given based on the theory and shown in Equation (7):

$$\Delta T_{ave}(\tau) = \frac{P_0}{\pi^{3/2} \cdot a \cdot k} \cdot D(\tau) \tag{7}$$

Where,

P_0 is the total output energy from the sensor;

a is the radius of the sensor disk;

k is the thermal conductivity of the sample; and

$D(\tau)$ is a dimensionless time-dependent function with

$$\tau = \sqrt{\frac{t}{\Theta}} \tag{8}$$

Where,

t is the measurement time; and

Θ is the characteristic time, expressed as:

$$\Theta = \frac{a^2}{\kappa} \tag{9}$$

Where,

κ is the thermal diffusivity of the sample.

a is the radius of the sensor disk

With all the equations above, the relationship between the recorded temperature increase and $D(\tau)$ could be built and it is easy to make a computational plot as shown in Equation (7). The plot would look like a straight line, the intercept of which is ΔT_i and the slope is $\frac{P_0}{\pi^{3/2} \cdot a \cdot k}$ after the experimental time is longer than Δt_i, What's more, because κ and Θ cannot be decided before test, an iteration method should be used to obtain the final straight line. Thus it is possible to get both thermal conductivity and thermal diffusivity from one single transient recording. (*Thermtest Inc., 2015; Bouguerra et al. 2001*) The specific heat can be obtained by Equation (10).

$$c = \frac{k}{\kappa} \tag{10}$$

Where,

k is the thermal conductivity of the sample;

κ is the thermal diffusivity of the sample.

3.2.3 Measurement Procedure

The measurement procedures are as follows:

(1) Set up samples. Make sure that sensor is sandwiched between two samples without any air gap.

(2) Input initial parameters, including temperature and maximum probing depth.

In TPS measurement, thermal conductivity is calculated based on an assumption that the sensor was located in an infinite medium, which means that any boundary condition of samples that influence thermal transport properties would interrupt the measurement. To avoid this boundary influence, the “available probing depth” must be defined before the test to indicate the shortest distance from the edge of spiral line in the sensor to the outside boundary of any sample, as shown in Figure 3-4. If the measured probing depth exceeds the acceptable probing depth, a warning would be pointed out in the final results. (*Thermtest Inc., 2015*)

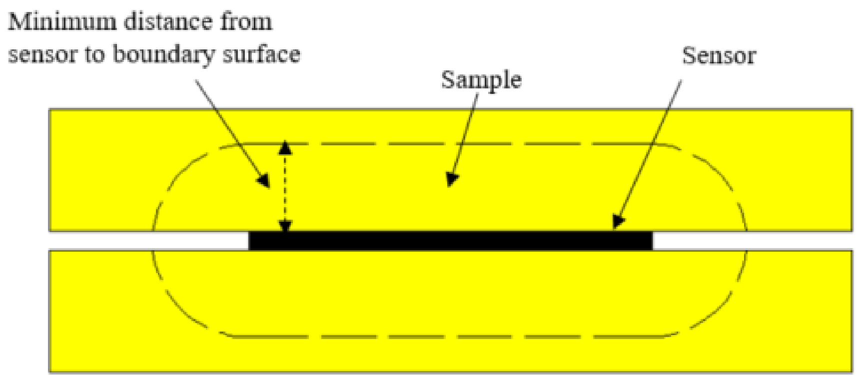

Figure3-4 Minimum distance from sensor to sample boundary surface (*Thermtest Inc., 2015*)

(3) Determine heating power and measurement time.

After defining the maximum probing depth, the measurement can be performed by given two parameters, the heating power and the measurement time. The heating power is the total constant thermal energy supplied to the sensor to increase its temperature, which would be affected by the thermal conductivity of samples and the size of sensor. For example, insulating material only needs a very small power, in the range of mW, but a high conductivity material, like metal, could require much higher heating power without damage the sensor. What's more, the smaller sensor allows relative lower heating power, while the larger sensor requires higher power. (*Thermtest Inc., 2015*)

Measurement time is the total measuring time of the experiment. By heating the sensor for a period of time (measurement time), heat wave would transport into sample. The probing depth is used to represent the thermal penetration depth, which is defined as shown in Equation (11).

$$d_p = 2\sqrt{\kappa \cdot t} \tag{11}$$

Where,

d_p is probing depth;

κ is thermal diffusivity;

t is measurement time.

It should be noted that the probing depth must be smaller than the available probing depth given before. And the ratio of total measuring time and characteristic time should be between 0.33 to 1, which means that the probing depth should between 1.15 and 2 times the radius of the sensor. (*Thermtest Inc., 2015*)

Because TPS test can only measure thermal properties within a relatively small volume, the sensor was put at different locations inside the sample to conduct parallel tests which can calculate average values, as shown in Figure 3-5.

(a) (b)

Figure3-5 TPS test on (a) cement paste; (b) aggregate

3.3 Heat Flow Meter Method

3.3.1 Test Setup

Because of the high heterogeneity of porous concrete, steady-state heat flow meter tests were conducted to measure the thermal conductivity of porous concrete samples following ASTM C518-17. The equipment used in the tests is TC2000 Heat Flow Meter, developed by XIATECH, Inc.

The heat flow meter is composed of cold plate, hot plate, guard plates, and heat flux transducers, as shown in Figure 3-6. The measurement ranged from 0.01~2 W/mK, with the precision of 0.001 W/mK and the accuracy of ±3%. The working plates of TC2000 are able to adjust normal pressure automatically to reach the maximum contact areas, reducing thermal resistance without crashing any part of samples. The guard plates were placed around heating plates to prevent thermal losses. All test data were processed by Heat Flow Meter 2.0 software, which is able to monitor the tests and calculate thermal properties.

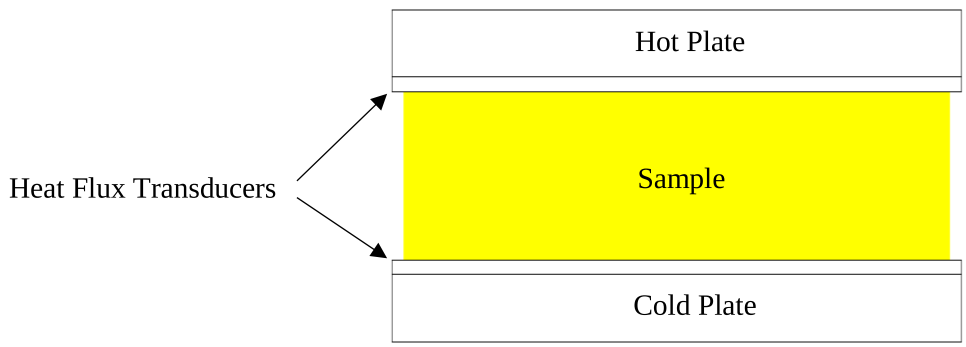

(a)

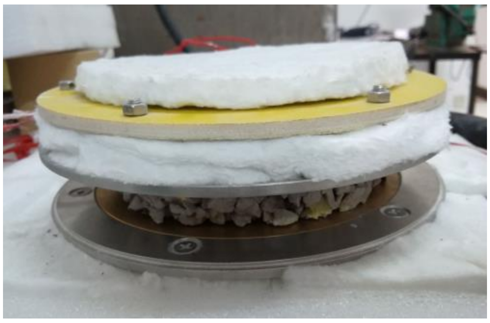

(b)

Figure 3-6 The Schematic diagram of the experiments (a) heat transfer mode (b) device setup

3.3.2 Measurement Principles

The heat flow meter method is a steady-state method to measure thermal properties of materials. Hot and cold plates sandwich the tested sample to generate temperature gradient within it. Heat flux transducers are placed between each plate and sample to measure the heat flux for further calculation. Guard plates are employed to lessen lateral heat losses applied on the tested sample to reach one-dimensional thermal stabilization. Based on Fourier's law, heat flux in one dimension is expressed in Equation (12). Since thermal conductivity and temperature gradient are stable during thermal steady state, the thermal conductivity can be calculated.

$$q = -k\frac{dT}{dy} \tag{12}$$

Where.

q is heat flux;

k is thermal conductivity; and

$\frac{dT}{dy}$ represents the temperature gradient in y direction.

3.4 Results and Analysis

3.4.1 Thermal Properties of Cement Paste

The thermal conductivity, thermal diffusivity, and specific heat of cement paste were measured using TPS tests. Twelve tests were conducted for each mix type by putting sensor at different locations of the samples. The statistical results are listed in Figure 3-7, 3-8, 3-9., respectively for thermal conductivity, thermal diffusivity, and specific heat. The column shows the average value of thermal property, while the error bar indicates one standard deviation of all 12 measurements. It is clear that the test results showing good repeatability and can represent the accurate properties of cement paste samples.

The PRC-3 and PRC-7 samples had almost the same w/c ratio, but a small amount of fly ash is added in PRC-7 to replace cement. The thermal conductivities of PRC-7 samples were found similar to PRC-3. *Kim et al.* (2003) found that fly ash would reduce the thermal conductivity of cement paste when 50% of fly ash is added to replace cement. By comparing PRC-3 with PRC-9, it could be concluded that w/c ratio can influence the thermal conductivity. With the increase of w/c ratio, the thermal conductivity of PRC-9 (w/c=0.33) is higher than that of PRC-3 (w/c=0.27)

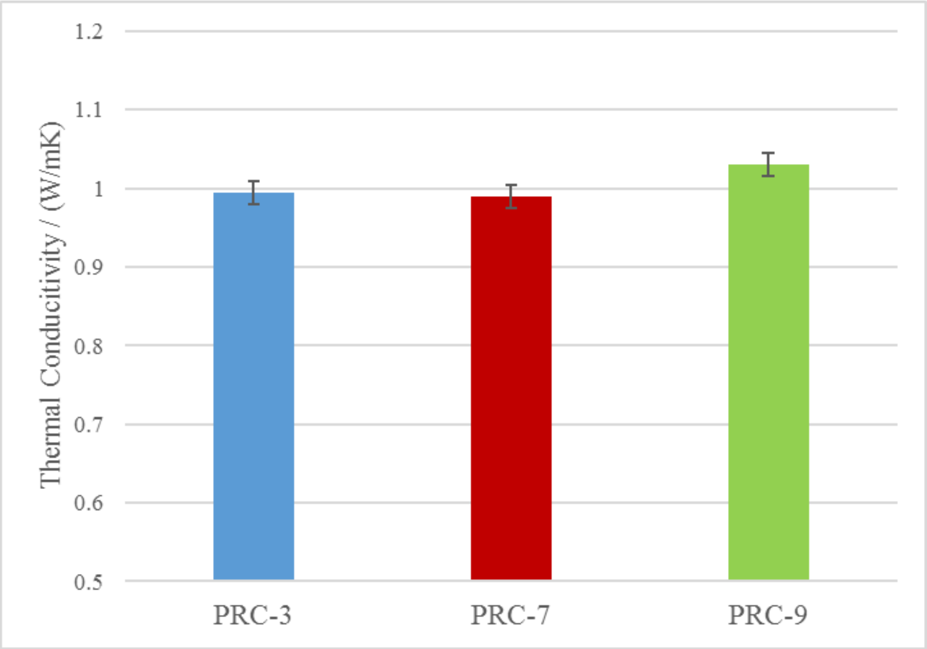

Figure 3-7 Thermal conductivity of cement pastes

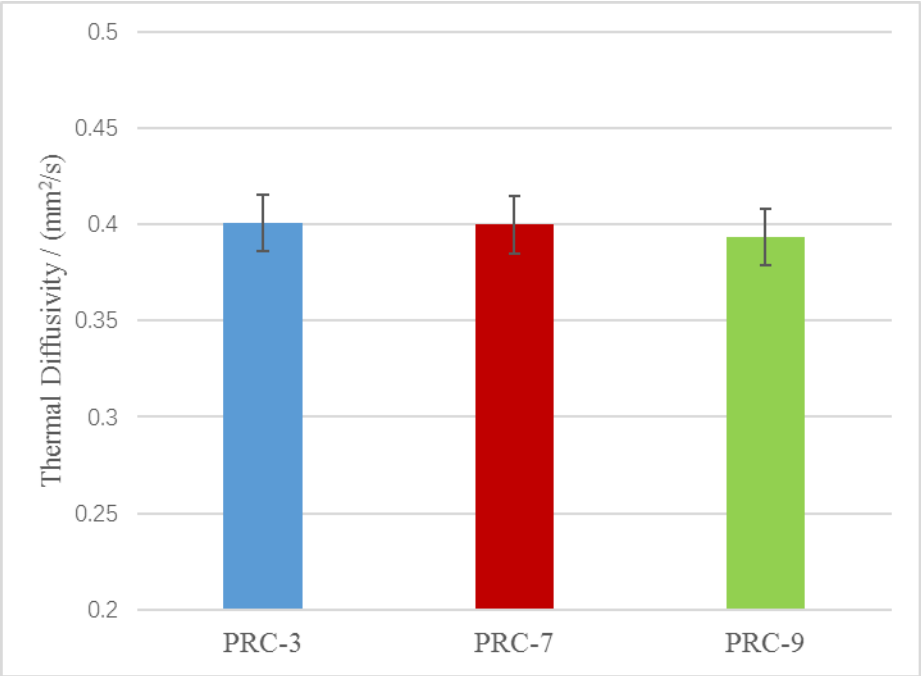

Figure 3-8 Thermal diffusivity of cement pastes

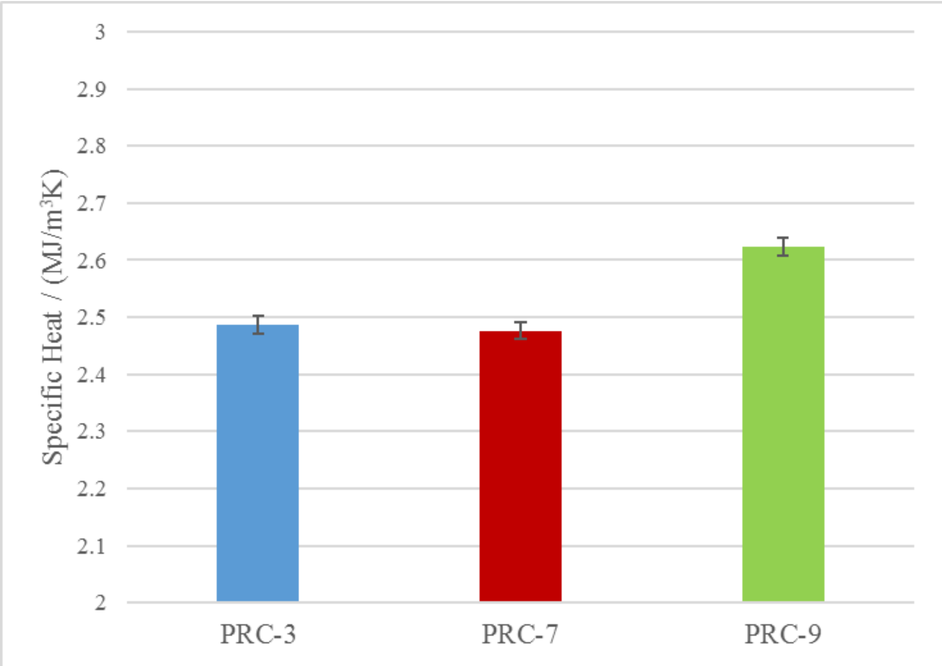

Figure 3-9 Specific heat of cement pastes

3.4.2 Thermal Properties of Aggregate

The TPS tests were also conducted to measure thermal properties of aggregates. Because of some subtle variations were observed, the mean value was calculated to represent the thermal conductivity thermal diffusivity and specific heat of aggregates, which are listed in Table 3.3.

Table 3.3 Summary of Thermal Properties of Aggregate

Thermal properties	Average	Standard Deviation
Thermal Conductivity (W/mK)	1.891	0.092
Thermal Diffusivity (mm^2/s)	0.866	0.107
Specific Heat (MJ/m^3K)	2.107	0.237

3.4.3 Thermal Properties of Porous Concrete Mixture

The porous concrete samples were measured by heat flow meter and the test results were plotted in Figure 3-10. Figure3-10 shows that for the same mix proportion, the thermal conductivities of porous concrete samples have large differences among different samples. The range of thermal conductivity for PRC-3 is from 0.4688 to 0.8135 W/mK, for PRC-7 is from 0.4944 to 0.7545 W/mK, and for PRC-9 is from 0.5281 to 0.8694 W/mK, respectively.

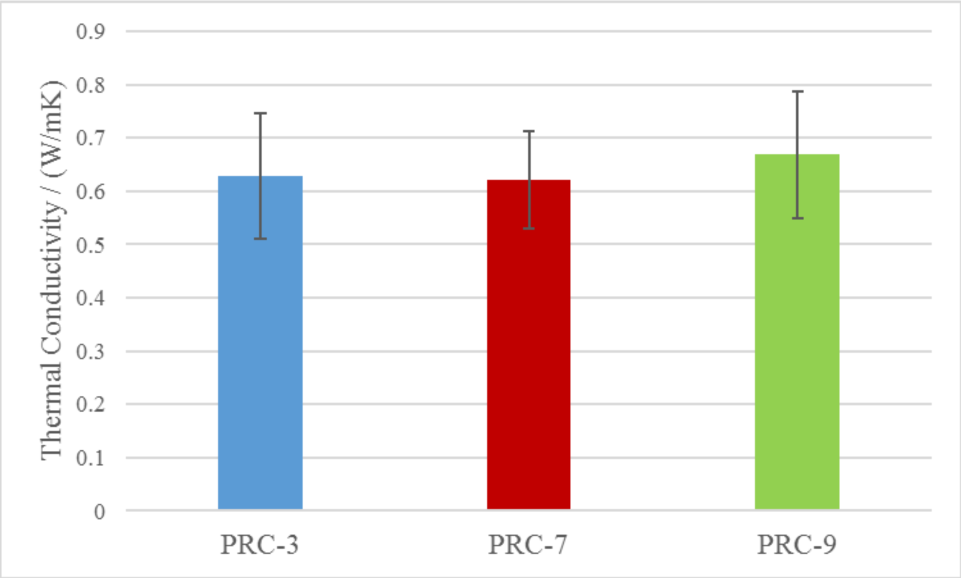

Figure 3-10 Thermal conductivity of porous concrete

The variation of thermal conductivity for the same mix design is relatively large due to the non-uniform distribution of inter-connected air voids within porous concrete, which usually happens when porosity is high such as 20%-40%. Although different sliced samples have the same mix proportion, their internal microstructures can be much different with each other. The heat flux in the porous concrete mainly transports through solid parts (cement and aggregate); while the heat channel will be interrupted by air voids due to the small thermal conductivity of air (0.025 W/mK). This indicates that the characteristics of air void distributions play an important role in thermal properties. For better understanding the effects of internal porous structures on thermal properties of porous concrete, Computer Tomography (CT) was carried out to rebuild the three-dimensional microstructure of porous concrete and analyze the characteristics of air voids in the next chapter.

CHAPTER 4. ANALYSIS OF AIR VOIDS AND ITS RELATIONSHIP WITH THERMAL PROPERTIES OF POROUS CONCRETE

4.1 Image Analysis of Porous Concrete

For detecting the internal structure of opaque materials, X-ray is often employed due to its excellent penetrability. X-ray is also called Roentgen radiation, named after its finder W.K. Roentgen, with the wave length range from 0.01nm to 10nm. The initial application of X-ray was medical only, then it was extended to industry use for non-destructive detection.

In order to investigate the relationship between air void characteristics and thermal properties of porous concrete, 18 samples were analyzed using X-ray computed tomography technique. The 3D images were imported into the image processing software. By means of choosing a proper threshold of gray value, the void and solid (including aggregates and cement paste) parts could be segmented and analyzed separately.

The cuboid sample was cut from each cylindrical sample to avoid edge effects on samples. The dimensions of cuboids were around 110 by 95 by 20 mm, which varied a little based on the dimension of cylindrical specimens. Figure 4-1 shows schematic illustrations of cuboid sample cut from cylindrical sample.

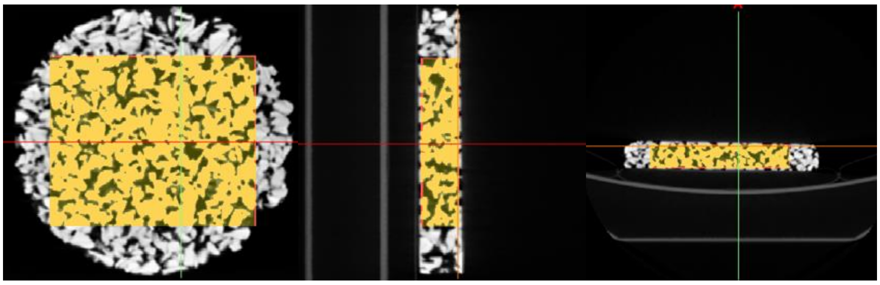

Figure 4-1 schematic illustrations of cuboid sample cut from cylindrical sample

Because of the complexity of microstructure, the centerlines of air voids were employed to study the characteristics of air void distribution, as shown in Figure 4-2. Because of high porosity, more than 97% of the air voids are connected and form net structures. The net structure was separated into single lines without any intersection to calculate the total length and distribution of each air void segment, with the junctions were represented by red dots. Meanwhile, a number of control points were interpolated along centerlines to provide detailed information about the characteristics of air voids, like coordinate, curvature, sectional areas, and so on. Usually, the distances between two control points are smaller than 0.9 mm.

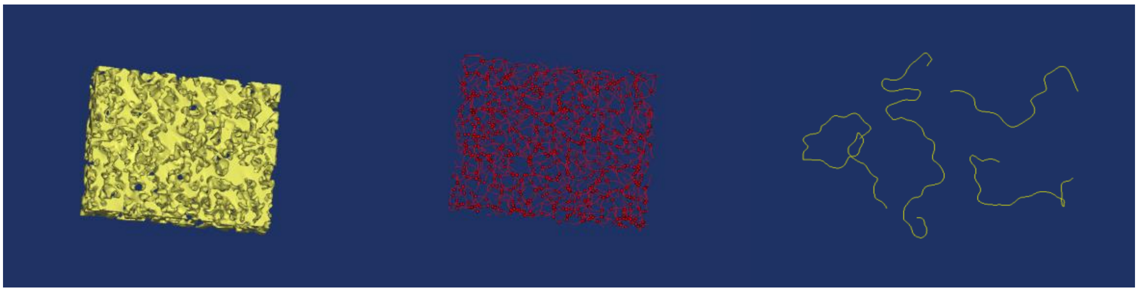

(a) (b) (c)

Figure 4-2 schematic of (a) all air voids; (b) centerlines of air voids; and (c) several separated centerlines

4.2 The Relationship between Porosity and Thermal Conductivity

4.2.1 Porosity

By setting a specific threshold value, the solid and air void can be distinguished from the scanned pictures and thus the respective volume can be calculated. The porosity of each cuboid sample, which is the volumetric ratio of air void and whole sample, is shown in Figure4-3, as well as the porosities of the intact 6'' by 12'' samples are also listed. Experimental results for PRC-3, PRC-7 and PRC-9 are 24.30%, 26.33% and 24.92% subsequently. The models' average porosities for PRC-3 and PRC-7 is 35.54% and 38.46% respectively, both of which have quite large variations, with standard deviation 0.052 and 0.061 correspondingly. The model's porosity for PRC-9 is relatively uniformly, with the average porosity and standard deviation as 37.60% and 0.017 respectively. One possible explanation for this variation can lay in the preparation procedures. Because of the large air void content of porous concrete, the blending can hugely affect the homogeneity of aggregate distribution, which can lead to a great discrepancy of microstructure. In addition, the flowing downward tendency of cement paste at curing process can result in the diversity of air voids between upper and lower parts of the same.

Besides, the porosity for PRC-9 samples is more uniform than PRC-3 and PRC-7 samples as the porosity changes. One possible explanation is that PRC-9 samples consist of smaller aggregates, which may reduce the variation of air void distribution in porous concrete. Due to all samples were cut from one 6'' by 12'' big cylindrical sample, their more uniformly porosity can be expected.

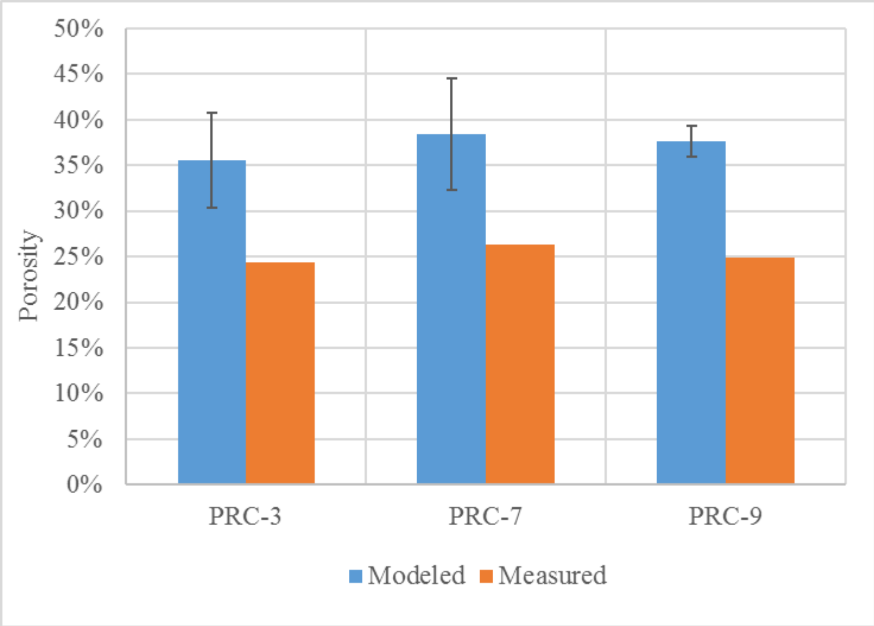

Figure 4-3 Porosity Variations of Porous Concrete Samples

The porosity calculated from image processing method differs notably from the tested value, which may be due to the selection of threshold value in image processing. However, the trend in the estimated porosity from image analysis should follow the one in the real specimen. Therefore, the relationship between porosity and microscopic structure can be still evaluated with image analysis. In the future study, the threshold value in the image analysis will be calibrated using the measured air void contents of thin layer samples.

4.2.2 Prediction of Thermal Conductivity of Porous Concrete

Considering the big difference of porosities among porous concrete samples, some analytical models were employed to build the relationship between porosity and thermal conductivity. Analytical models are commonly used to estimate thermal conductivity of heterogeneous composite material, because of their physical basis, rapid calculation, and rational accuracy. (Wang et al. 2006). Series model and parallel model are broadly considered as the minimum and maximum limits of effective thermal conductivity (ETC) for two phase's system. Series model and parallel model (J. K Carson 2016) refer to the solid and the fluid phase are in layers normal and parallel to the direction of heat flow, respectively.

If we assume that phases are randomly distributed, ETC could be calculated by geometric mean model. Maxwell-Eucken model predicts the ETC of a continuous matrix with some distinct particles inside. (Hashin and Shtrikman, 1962) These particles are far enough that temperature distortion of each particle would not influence others. Effective medium theory (EMT) model is used for more general situation, estimating a completely random distributed system. (R. Landauer,1952) Woodside and Messmer also suggest a model to predict ETC of porous media which is a combination of series and parallel model. (I.H. Tavman 1996) Table 4.1 listed all the equations of the aforementioned model and their parameters.

Table 4.1 Five effective thermal conductivity models for two-phase materials

Model	Effective thermal conductivity equation
Series Model	$k_e = \frac{k_s \cdot k_f}{\varepsilon \cdot k_s + (1-\varepsilon) \cdot k_f}$ (13)
Parallel Model	$k_e = \varepsilon \cdot k_f + (1-\varepsilon) \cdot k_s$ (14)
Maxwell-Eucken Model	$k_e = k_f \cdot \frac{2\varepsilon \cdot k_f + (3-2\varepsilon) \cdot k_s}{(3-\varepsilon) \cdot k_f + \varepsilon \cdot k_s}$ (15)
EMT model	$\varepsilon \cdot \frac{k_f - k_e}{k_f + 2k_e} + (1-\varepsilon) \cdot \frac{k_s - k_e}{k_s + 2k_e} = 0$ (16)

Woodside and Messmer Model	$$k_e = \frac{a \cdot k_s \cdot k_f}{k_s \cdot (1-d) + d \cdot k_f} + c \cdot k_f \qquad (17)$$ $$c = \varepsilon - 0.03,\quad a = 1 - c,\quad d = \frac{1-\varepsilon}{a}$$
k_e is effective thermal conductivity; k_s is the thermal conductivity of solid phase; k_f is the thermal conductivity of fluid phase; ε is the porosity.	

The 18 tested samples were verified by these analytical models and the results were drawn below:

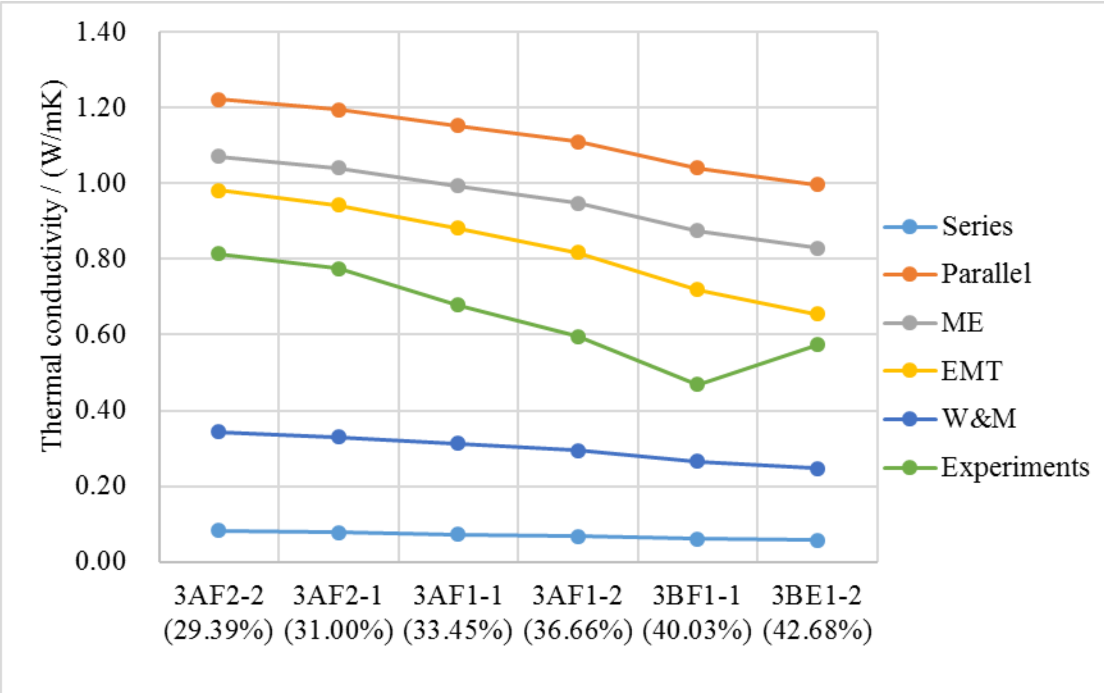

(a)

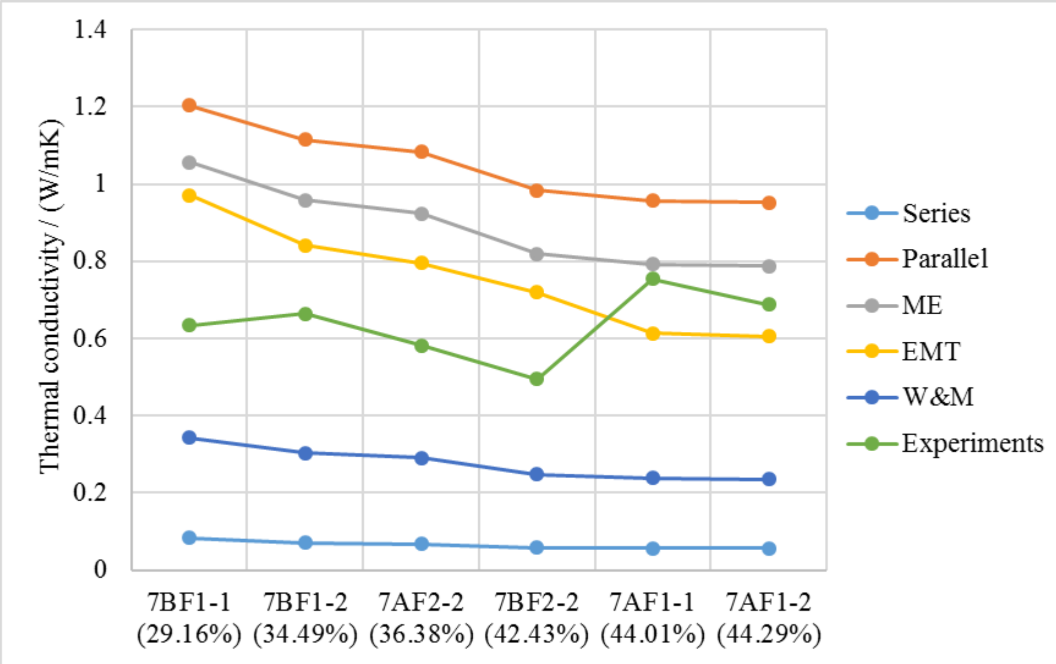

(b)

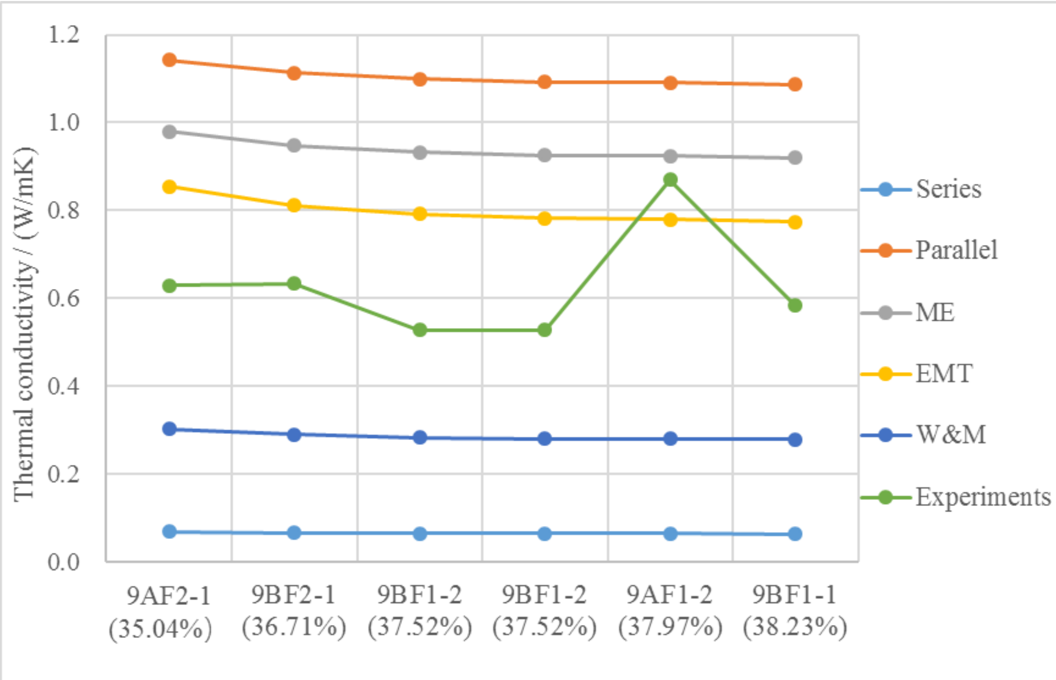

(c)

Figure 4-4 The thermal conductivity of porous concrete with design mix (a) PRC-3; (b) PRC-7; and (c) PRC-9

The results show that the parallel and series models form the upper and lower boundary for prediction values of thermal conductivity. The results predicted by other models and experimental measurements were all fall in this region, varying with porosities. For porous concrete with high porosity, the predicted results can be ranked as Parallel > ME > EMT > W&M > Series model. All analytical models have the same trend when the porosity changes, although the specific values are different. With the increase of porosity for the same mix proportion, the predicted thermal conductivity decreases, which does not have a very good consistency with the experimental results. These analytical models simply calculate the thermal conductivity based on the volumetric fractions of different components, without considering the microscopic structure or the distribution of air voids in porous concrete. As a result, they are not appropriate to predict the properties of highly heterogeneous materials, like porous concrete.

4.3 Characteristics of Air Voids in Porous Concrete

4.3.1 Pore Length and Directional Distribution

It is expected that the interconnected air voids have different distribution patterns in different directions. In order to evaluate the directional variation of air void, the accumulated total length of centerlines of air voids and its projections at different directions were calculated. Because the lengths in three directions of cuboid samples are different, the concept of normalized length is used, which is defined as the ratio of directional length of air voids to the sample's volume.

Figure 4-5 (a) and (b) show the normalized length ratio of air voids, respectively, for three different mix designs of porous concrete (PRC-3, PRC-7, and PRC-9). In the Figure, x and z directions are two orthogonal axes in the horizontal surface and y direction is normal to horizontal surface.

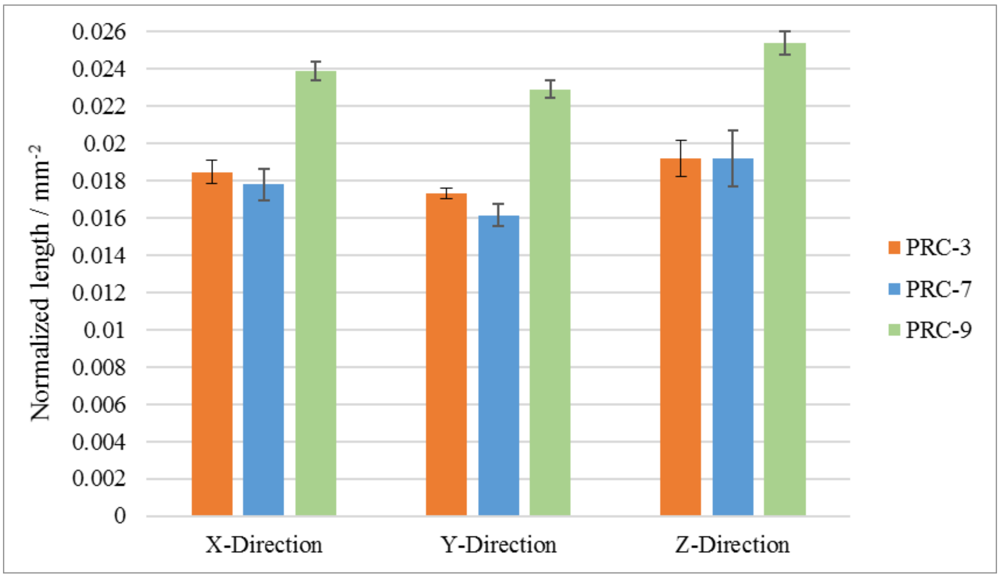

(a)

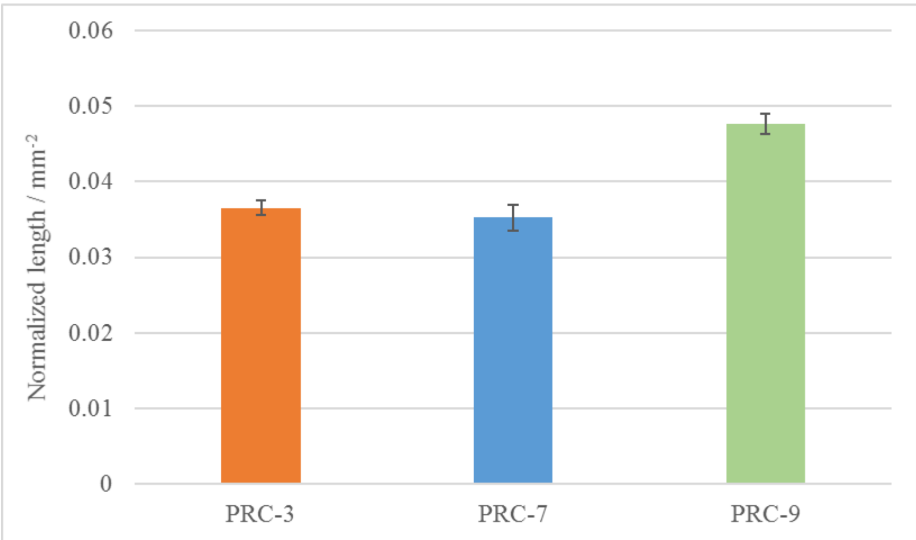

(b)

Figure 4-5. Comparison of normalized pore lengths for the samples within design mix: (a) length along different directions; and (b) total length

From the Figure 4-5 (a), the x component of normalized length is almost the same as z component of normalized length, which are both larger than the length along y direction.

This trend indicates that air voids are not totally randomly distributed within porous concrete. Within the horizontal surface, slight differences indicates random distribution of air void, while the connected voids in vertical direction are always less than that in horizontal direction. Several explanations can be proposed for this phenomenon, like gravity impact or molding methods during laboratory preparation of concrete specimen. Figure 4-5 (b) illustrates the normalized total length ratio for three types of porous mix. The total length of PRC-9 is significantly higher than that of PRC-3 and PRC-7, which may result from the smaller aggregates employed in PRC-9. Compared with large aggregates, small aggregates are more easily to form small air voids. Under the condition of similar porosity, the smaller the aggregates' section area, the longer the air void connecting length.

4.3.2 Pore Shapes and Sizes

The ellipticity was employed to show the shape characteristics of air void in cross sections. It represents the best-fit ellipse for the cross section of air void at the control point. The ellipticity can be calculated based on equation below:

$$E = \sqrt{\frac{R_1^{\,2} - R_2^{\,2}}{R_1^{\,2}}} \tag{18}$$

Where,

R_1 is the largest radius of ellipse;

R_2 is the smallest radius of ellipse.

Figure 4-6 (a), (b) and (c) show the probability distribution of ellipticity of air voids for each porous concrete sample. The highest probability shows up when the ellipticity is around 0.9. Because the ellipticity varies within 0 to 1 and the higher ellipticity represents the voids are more slender. Thus it can be concluded that the shape of air voids within porous concrete tend to be slender than round.

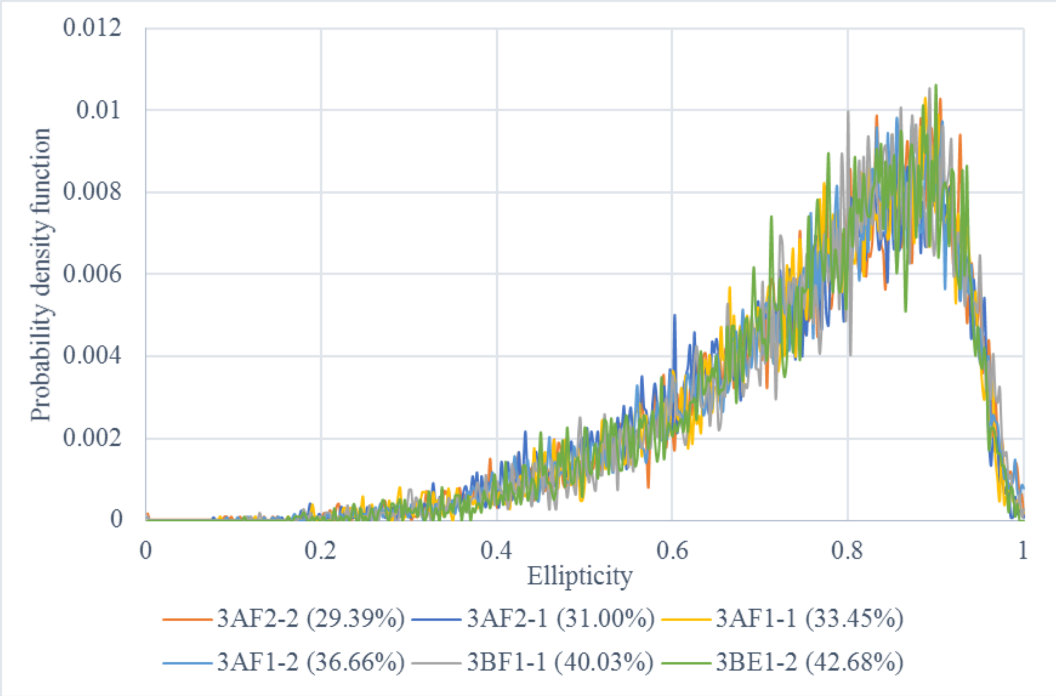

(a)

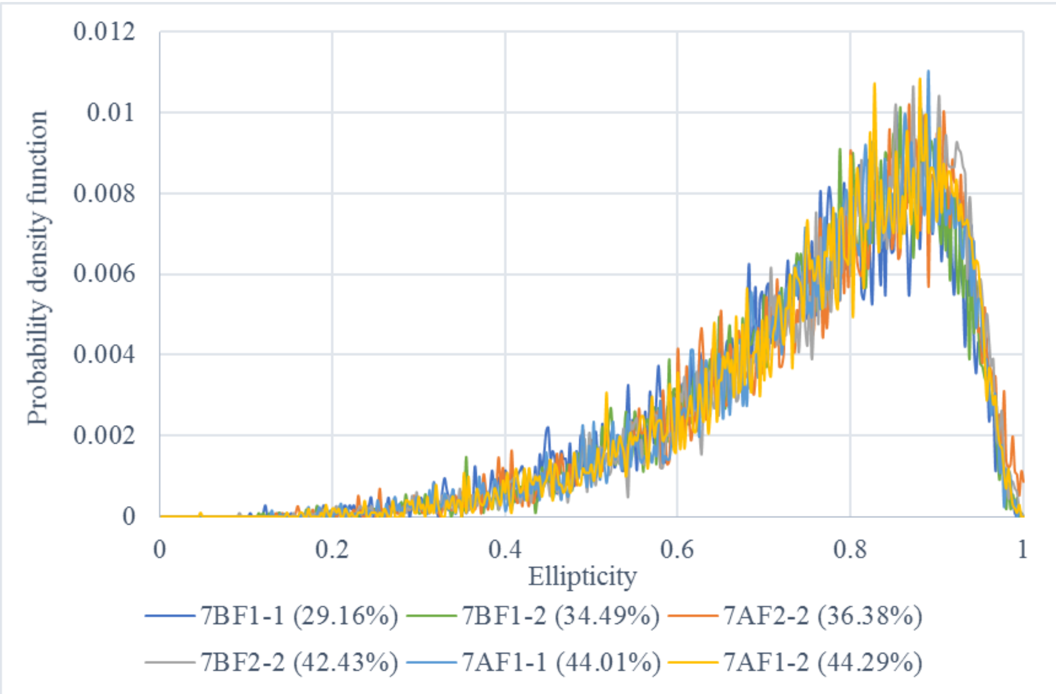

(b)

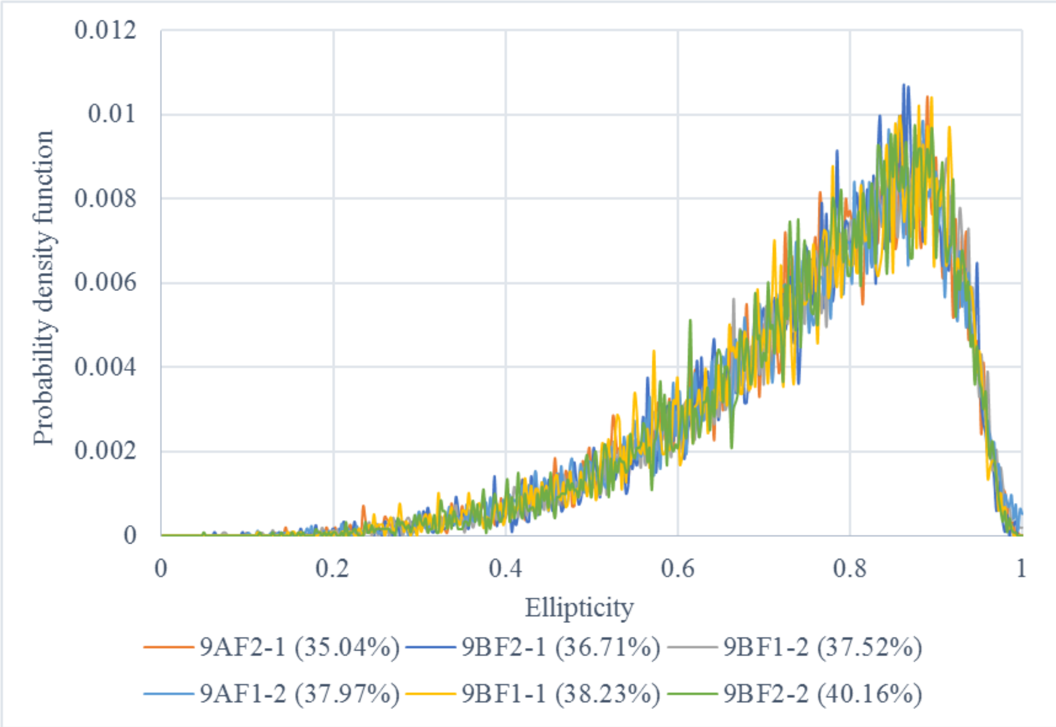

(c)

Figure 4-6 The probability density function of ellipticity of air voids for the sample with design mix (a) PRC-3; (b) PRC-7; and (c) PRC-9

Figure 4-7 shows the cumulative distribution function of ellipticity for all the pore cross sections. The distribution functions of all samples are very similar, indicating that there might be not apparent relationship between ellipticity and porosity or aggregate microscopic structures.

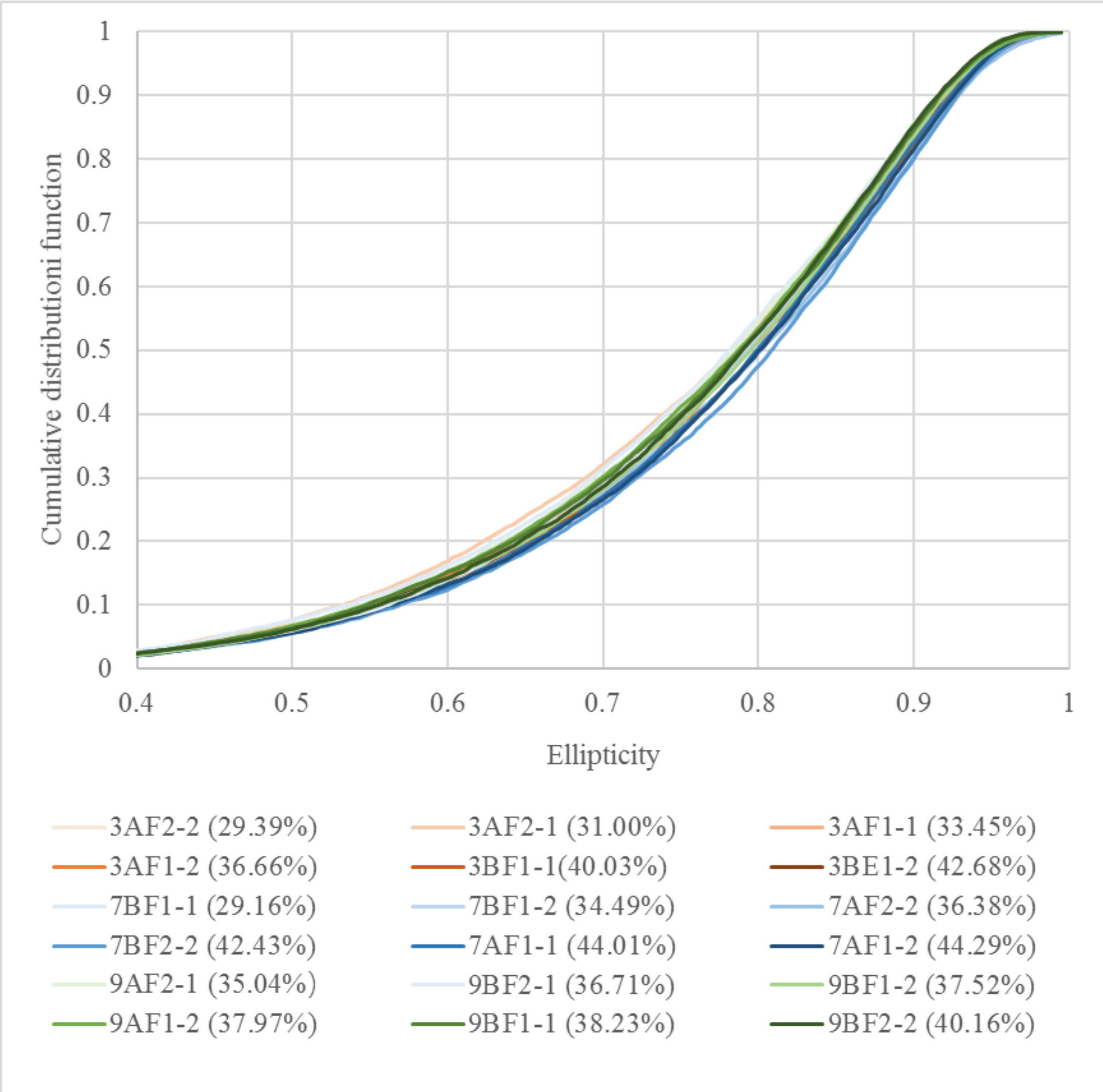

Figure 4-7 Ellipticity of air void

Figure 4-8 shows the cumulative probability distribution of effective air void diameter at each control point along the centerlines of air voids. The effective air void diameter is defined as the diameter of a circle which has the same area with the cross-section of air void at control point. The red, blue and green color curve represents PRC-3, PRC-7 and PRC-9 group respectively, and darker color means larger air voids. The results show that despite different mix proportion for three experimental groups, the effective air void diameter increases with the air void content in general, while the influence of w/c ratio and aggregate size is not that clear. In future studies, more experimental groups should be employed to investigate the influence of other factors.

Take PRC-3 for example, for 3AF2-2, which has the least air void content, 29.4%, the 90^{th} percentile of effective air void diameter is about 11mm. However, for 3AF1-2 and 3BF1-1 with air void contents of 36.8% and 40% respectively, the corresponding 90^{th} percentile values are 17mm and 20mm, respectively. Similar patterns can be found for PRC-7 and PRC-9.

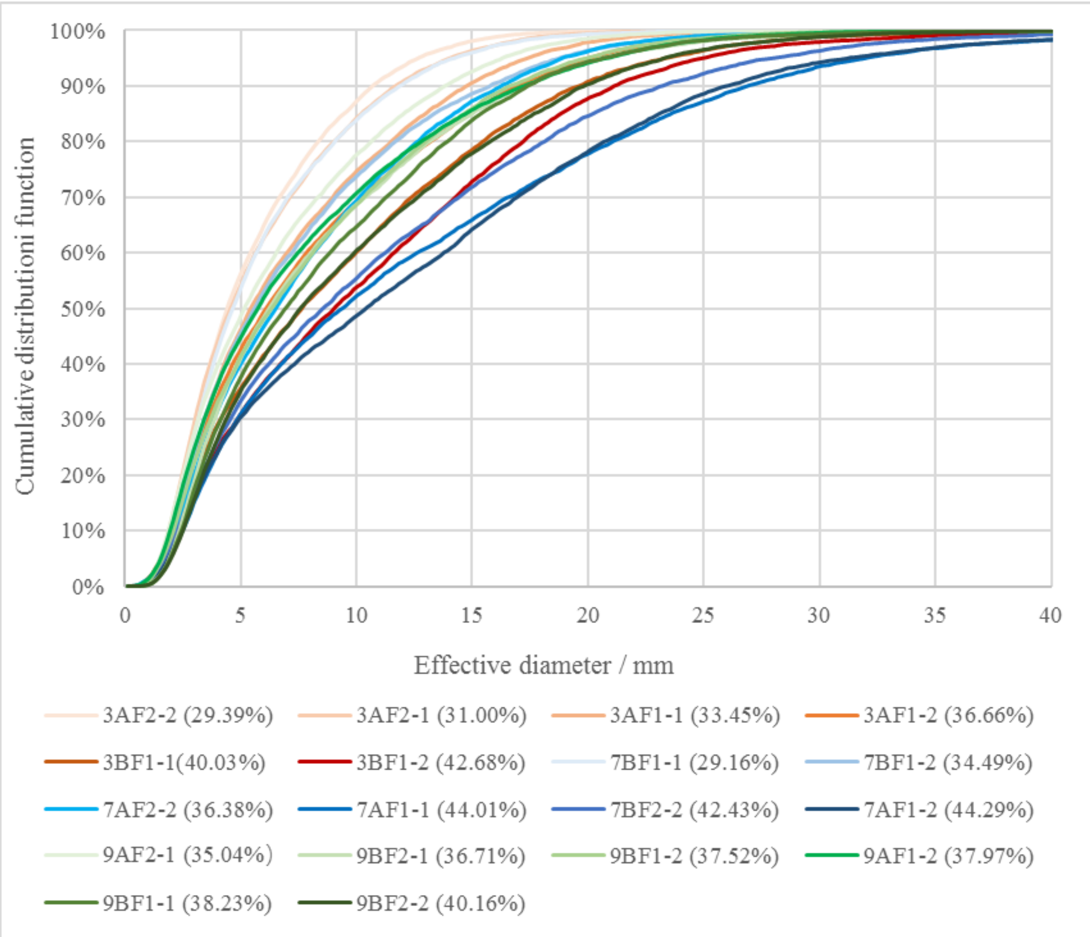

Figure 4-8 Equivalent diameter of air void

4.3.3 Pore Tortuosity and Curvature

Tortuosity is employed to analyze the characteristic of porous concretes, which is defined by Equation (19):

$$\tau = \frac{L}{C} \tag{19}$$

Where,

L is the length of the curve;

C is the distance between two ends

As mentioned before, the connected air voids were separated into a number of segments. Tortuosity is calculated as the curve length of each segment over its distance between two ends. Figure 4-9 (a), (b) and (c) show the tortuosity of porous concrete with mix proportion PRC-3, PRC-7 and PRC-9, respectively. Among them, the highest probability is shown up around 1.01 to 1.03. The similar trend can be seen from all samples.

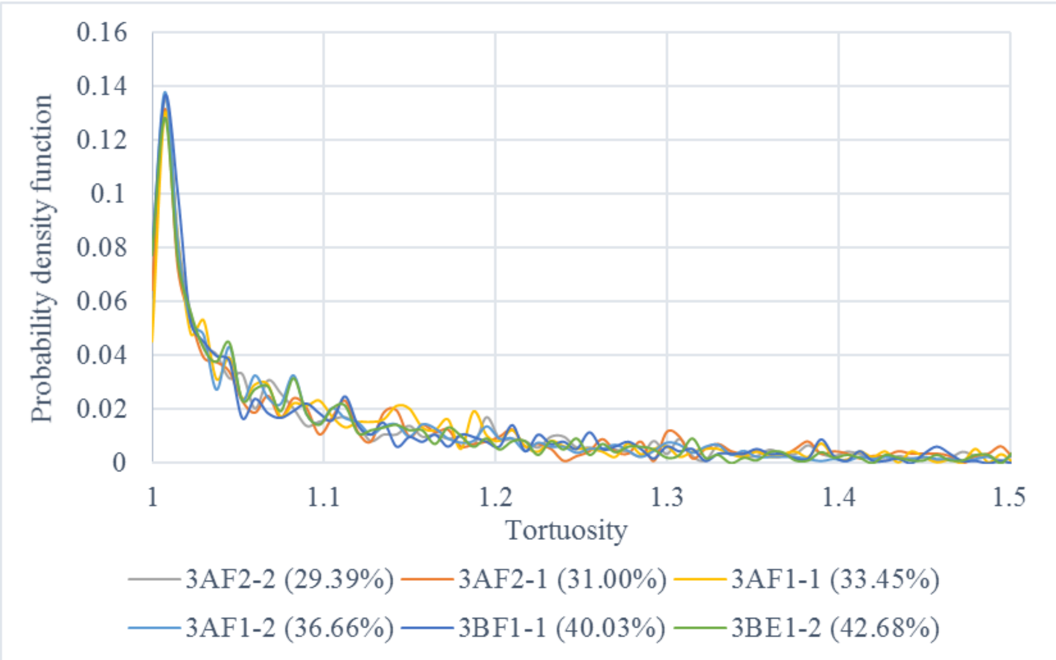

(a)

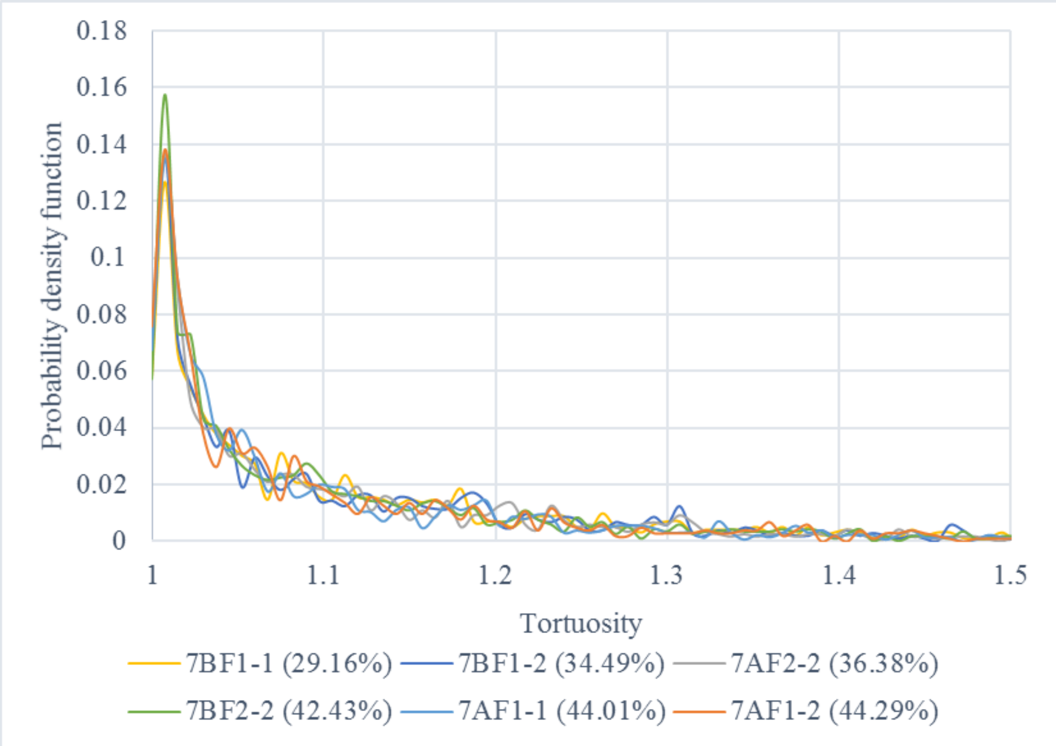

(b)

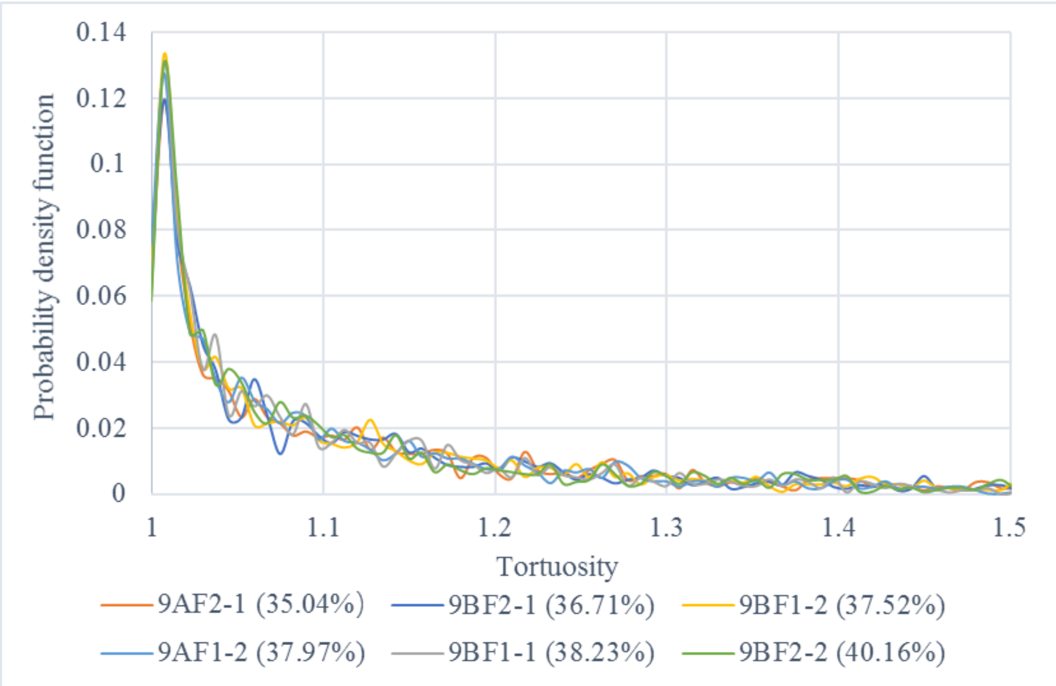

(c)

Figure 4-9 The probability density function of Tortuosity of air voids for the sample with design mix (a) PRC-3; (b) PRC-7; and (c) PRC-9

Figure 4-10 illustrates the cumulative distribution of air voids within all porous concrete samples. Over 90 percent of air voids segments have a tortuosity smaller than 1.35. However, these segments are very short, with an average length around 6mm. The direction of air void segments are quite easy to change, which also have a significant impact on the tortuosity of whole pores. As a result, in addition to tortuosity, the curvatures of air voids were also analyzed.

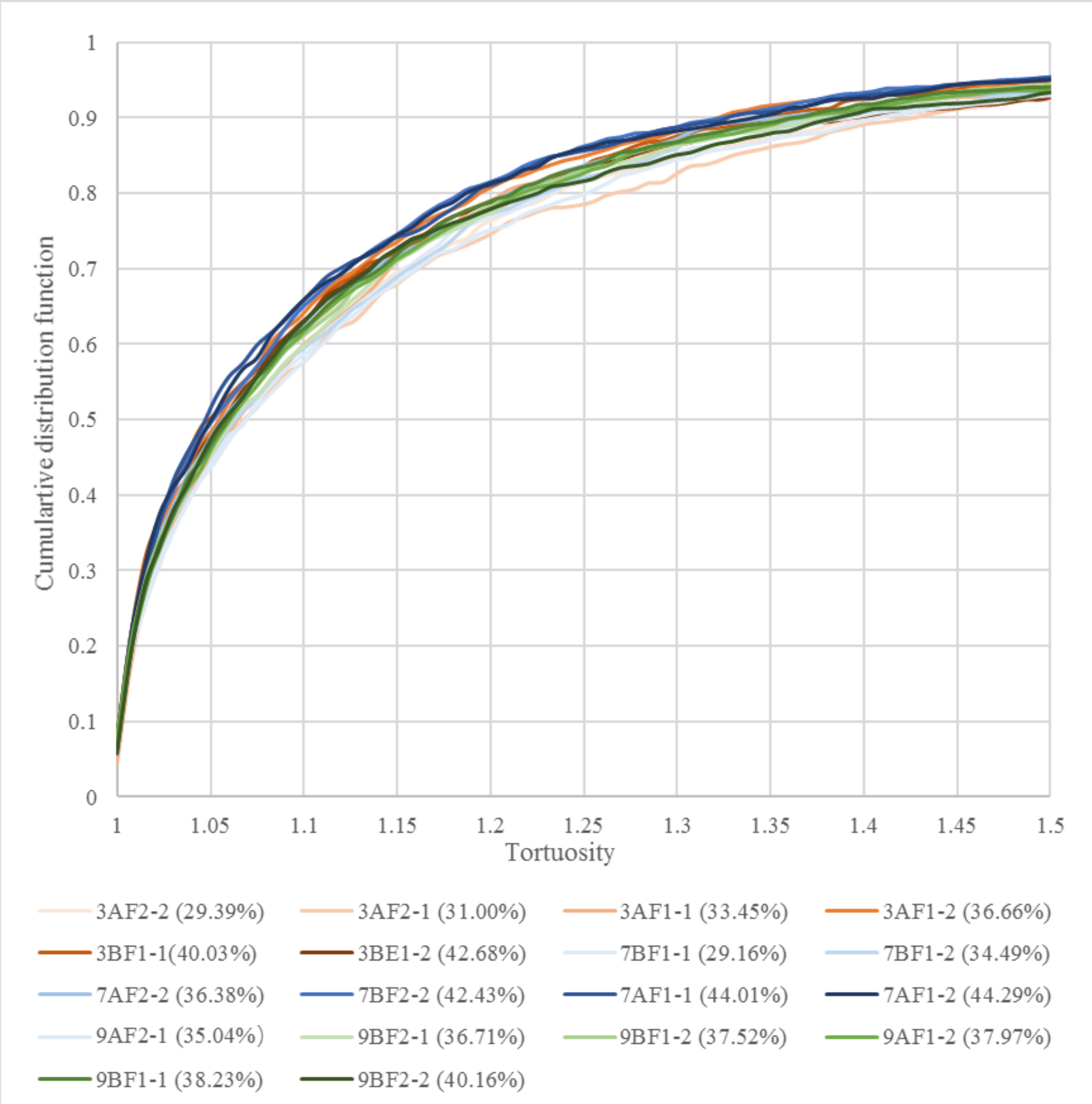

Figure 4-10 Tortuosity of air voids

Curvature is another index to represent the tortuosity of air void in porous concrete, which is defined as the reciprocal of radius of osculating circle at control points. Figure 4-11 (a), (b) and (c) present the curvature for porous concrete samples. Among them, the highest probability is shown up around 0.1 to 0.3. The similar trend can be seen from all samples.

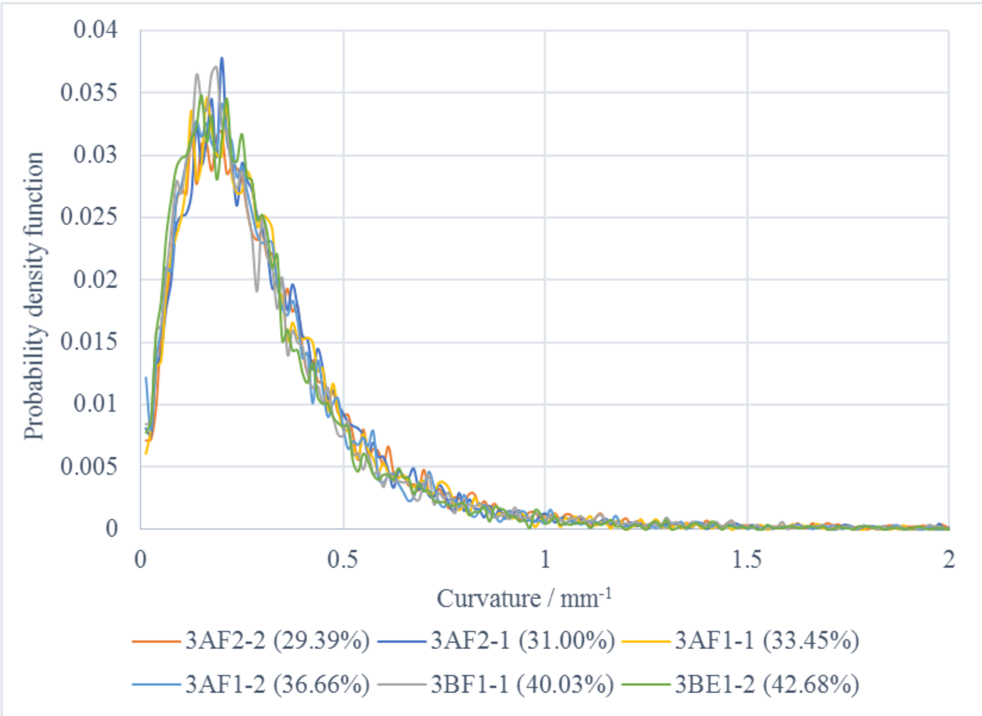

(a)

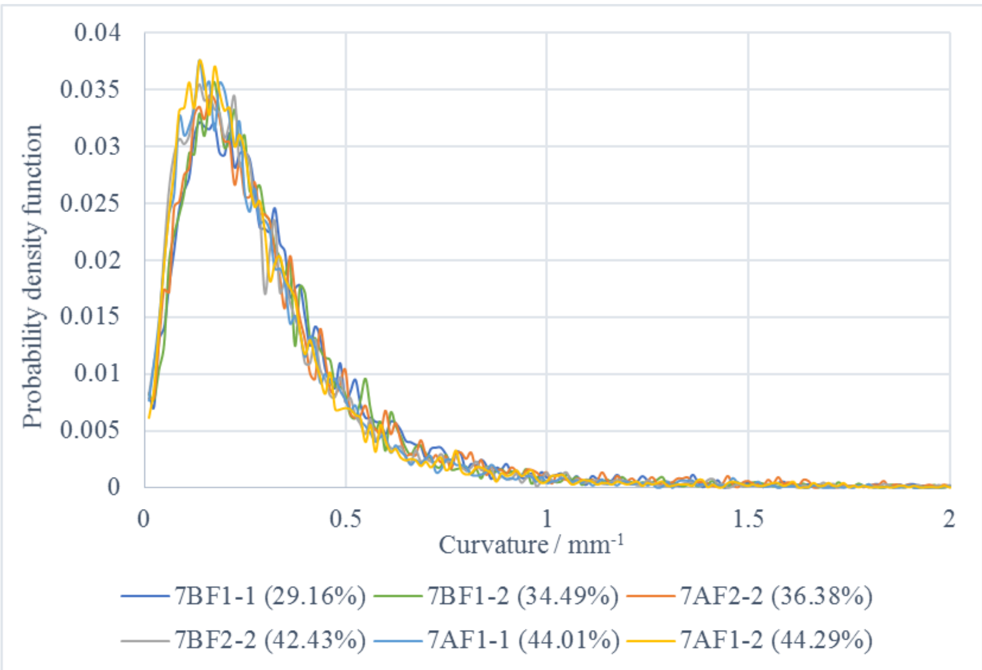

(b)

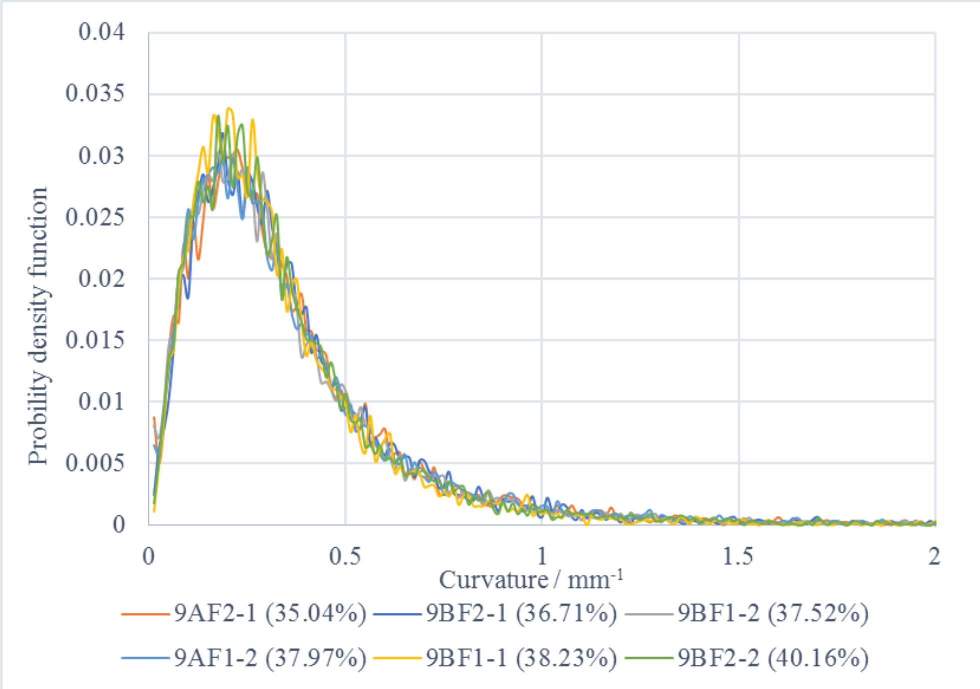

(c)

Figure 4-11 The probability density function of curvature of air voids for the sample with design mix (a) PRC-3; (b) PRC-7; and (c) PRC-9

Figure 4-12 illustrates the cumulative distribution of pore curvatures at control points. For the same mix design, the curvatures of air voids increase with the increasing of porosity. Take PRC-7 for example, for 7BF1-1, which has the least air void content, 29.16%, the 80th percentile of effective air void diameter is about 0.45 mm^{-1}. However, for 7AF1-1 and 71F1-2 with air void contents of 44.01%% and 44.29% respectively, the corresponding 80th percentile value are both around 0.39 mm^{-1}. Similar patterns can be found for PRC-3 and PRC-9.

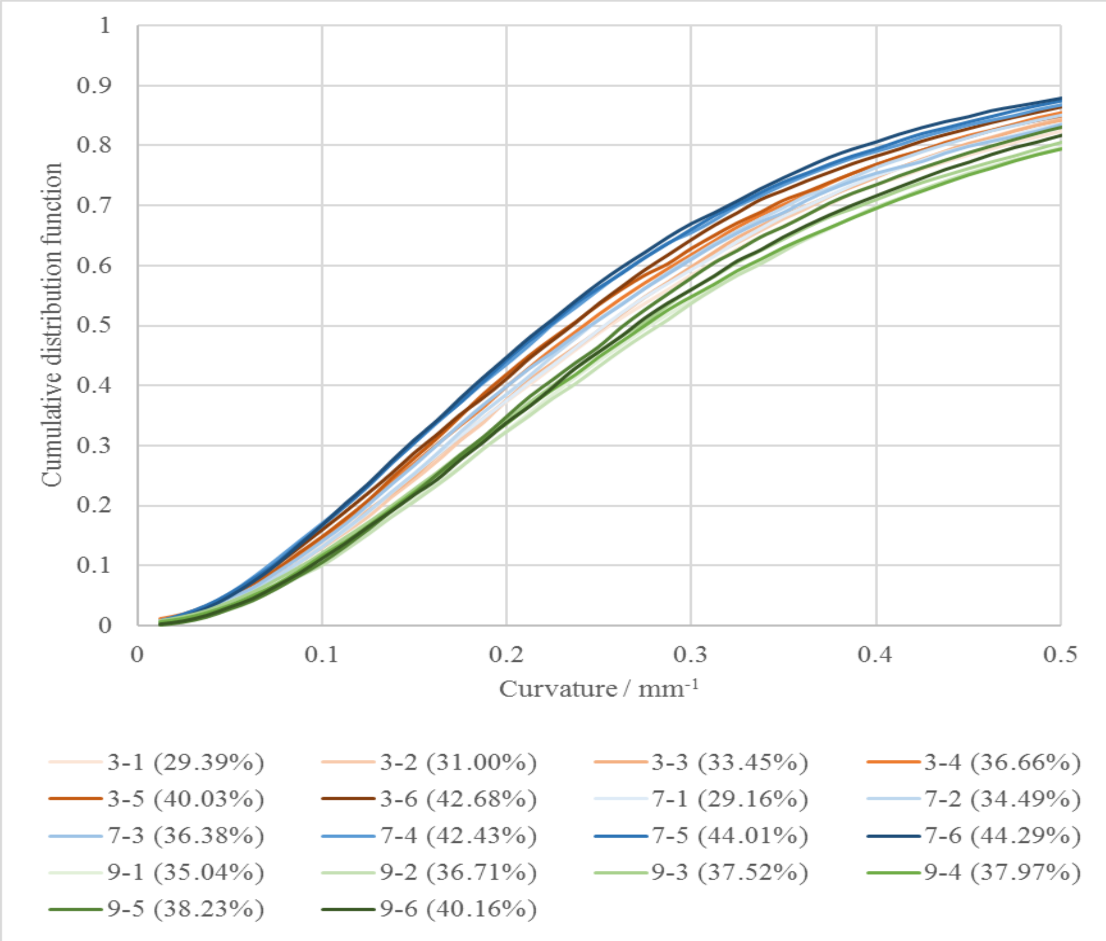

Figure 4-12 Curvature of air void

Besides, the pore curvatures of PRC-9 samples were found greater than those of other two groups. As the PRC-9 samples are composed of smaller aggregates, it indicates that the air voids between smaller aggregate can be more curved in the direction of pore and thus have the greater curvatures. The microscopic structure of air voids can change at a relatively short distance around small sized aggregates. For example, as shown in Figure 4-13, at the five control points, the aggregate particles with smaller sizes forms more tortuous air voids; while the larger sized aggregates result in relatively small curvature for the surrounding air voids.

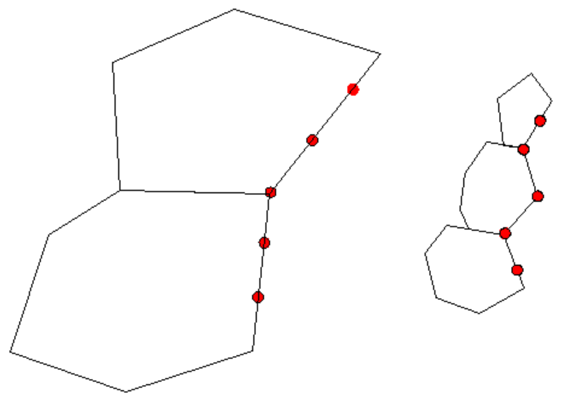

Figure 4-13 Schematic of different size of aggregates

CHAPTER 5. CONCLUSION AND FUTURE WORK

5.1 Findings and Conclusions

This thesis focused on evaluation of thermal properties and air void characteristics of porous concrete. The thermal properties of aggregates, cement pastes and porous concrete were measured by transient plate method (TPS) and steady state heat flow meter method, respectively. X-ray computed tomography (CT) technique was utilized and 3-D images were processed to analyze air void characteristics. The thermal properties of porous concrete were predicted using existing analytical models and compared to experimental measurements.

1. The thermal conductivity and specific heat of cement pastes increases as water cement ratio increases. Meanwhile, for the same mix design, the thermal properties of different cement paste samples had few variations.

2. The porous concrete is very heterogeneous and the same mix design cannot ensure the similar porosity; instead significant variations of porosity were observed.

3. The existing analytical results did not show satisfactory prediction results of thermal conductivity as compared to testing results. This indicates that the existing models are not suitable to predict the thermal conductivity of porous concrete. This is because the models ignore the complex microscopic structures of porous concrete.

4. Within the horizontal plane of cylindrical sample, slight differences of normalized projected lengths of air voids were observed in the orthogonal horizontal directions; while the normalized projected length of connected voids in vertical direction was

found smaller than those in horizontal directions. The smaller aggregates tend to form the longer air void length in porous concrete.

5. The curvature of air voids for smaller aggregates are greater than that of larger aggregates. Meanwhile, within the same mix design, the curvature of air voids increases with the increasing of porosity.

6. The porosity and aggregate size do not have significant influences on the ellipticity and tortuosity of air voids within porous concrete. However, with the increase of porosity, the air voids tend to have the greater equivalent diameter.

5.2 Recommendation for Future Work

The microstructure of porous concrete is complicated and well worth further research for building a structure-property relationship. Several aspects can be investigated in future research for better understanding of porous concrete.

1. This study only employed single sized aggregates within porous concrete. The gradation of aggregates can also affect the air void characteristics and distributions. More aggregate sizes and gradations should be considered in future work.

2. Due to the complicity of the structure of porous concrete, numerical modeling should be conducted to analyze the effect of air void characteristics on thermal properties in addition to experimental measurements.

3. The effects of air void characteristics on mechanical and hydraulic properties of porous concrete should be analyzed together with thermal properties.

REFERENCES

Aboufoul, M., and Garcia, A. (2016). "Factors affecting hydraulic conductivity of asphalt mixture." *Materials and Structures*, 50(2).

Assael, M. J., Antoniadis, K. D., Metaxa, I. N., Mylona, S. K., Assael, J.-A. M., Wu, J., and Hu, M. (2015). "A Novel Portable Absolute Transient Hot-Wire Instrument for the Measurement of the Thermal Conductivity of Solids." *International Journal of Thermophysics*, 36(10-11), 3083–3105.

Batool, F., and Bindiganavile, V. (2017). "Air-void size distribution of cement based foam and its effect on thermal conductivity." *Construction and Building Materials*, 149, 17–28.

Bentz, D. P. (2007). "Transient plane source measurements of the thermal properties of hydrating cement pastes." *Materials and Structures*, 40(10), 1073–1080.

Bouguerra, A., Aït-Mokhtar, A., Amiri, O., and Diop, M. (2001). "Measurement of thermal conductivity, thermal diffusivity and heat capacity of highly porous building materials using transient plane source technique." *International Communications in Heat and Mass Transfer*, 28(8), 1065–1078.

Brütting, M., Hemberger, F., Vidi, S., Wachtel, J., Mehling, H., and Ebert, H. (2016). "Determination of heat capacity by means of longitudinal guarded comparative calorimeter – Correction methods." *International Journal of Thermal Sciences*, 100, 423–429.

Carson, J. K. (2017). "Use of simple thermal conductivity models to assess the reliability of measured thermal conductivity data." *International Journal of Refrigeration*, 74, 458–464.

Chen, J., Wang, H., and Li, L. (2015). "Determination of Effective Thermal Conductivity of Asphalt Concrete with Random Aggregate Microstructure." *Journal of Materials in Civil Engineering*, 27(12), 04015045.

Crouch, L., Cates, M., Dotson, V., Honeycutt, K., and Badoe, D. (2003). "Measuring the Effective Air Void Content of Portland Cement Pervious Pavements." *Cement, Concrete and Aggregates*, 25(1), 11229.

Dasgupta, T., and Umarji, A. (2007). "Thermal properties of MoSi2 with minor aluminum substitutions." *Intermetallics*, 15(2), 128–132.

Dehdezi, P. K., Hall, M. R., Dawson, A. R., and Casey, S. P. (2013). "Thermal, mechanical and microstructural analysis of concrete containing microencapsulated phase change materials." *International Journal of Pavement Engineering*, 14(5), 449–462.

Fenollera, M. C. A. D., Míguez, J., Goicoechea, I., and Lorenzo, J. (2015). “Experimental Study on Thermal Conductivity of Self-Compacting Concrete with Recycled Aggregate.” *Materials*, 8(7), 4457–4478.

Fu, Xuli, and D. D.L., Chung. (1999). “Effect of Admixtures on Thermal and Termo-mechanical Behavior of Cement Paste.” *ACI Materials Journal*, 96(4).

Guntakal, S. N., and Selvan, S. (2017). “Application Of Pervious Concrete For Pavements: A Review.” *RASĀYAN Journal of Chemistry*.

Hashin, Z., and Shtrikman, S. (1962). “A Variational Approach to the Theory of the Effective Magnetic Permeability of Multiphase Materials.” *Journal of Applied Physics*, 33(10), 3125–3131.

Hot Disk Thermal Constants Analyser Instruction Manual. (2015). Hot Disk Thermal Constants Analyser Instruction Manual, Thermtest Inc., Fredericton, New Brunswick.

Kennedy, C. A., and White, M. A. (2005). “Unusual thermal conductivity of the negative thermal expansion material, ZrW2O8.” *Solid State Communications*, 134(4), 271–276.

Khan, M. (2002). “Factors affecting the thermal properties of concrete and applicability of its prediction models.” *Building and Environment*, 37(6), 607–614.

Khan, M.i. "Factors affecting the thermal properties of concrete and applicability of its prediction models." *Building and Environment* 37, no. 6 (2002): 607-14.

Kim, K.-H., Jeon, S.-E., Kim, J.-K., and Yang, S. (2003). “An experimental study on thermal conductivity of concrete.” *Cement and Concrete Research*, 33(3), 363–371.

Kočí, V. C. C., Maděra Jiří, Jerman Miloš, Trník Anton, and Černý Robert. (2012). “Computational analysis of a modified guarded hot plate experiment.”

Krishnamoorthy, R. R., David, T. K., Mastor, N. A. B., and Nadarasa, K. (2016). “Repair of Deteriorating Pavement Using Recycle Concrete Materials.” *Procedia Engineering*, 142, 371–382.

Landauer, R. (1952). “The Electrical Resistance of Binary Metallic Mixtures.” *Journal of Applied Physics*, 23(7), 779–784.

Lee, J.-H. (2017). “Influence of concrete strength combined with fiber content in the residual flexural strengths of fiber reinforced concrete.” *Composite Structures*, 168, 216–225.

Li, H., Harvey, J. T., Holland, T. J., and Kayhanian, M. (2013). “The use of reflective and permeable pavements as a potential practice for heat island mitigation and stormwater management.” *Environmental Research Letters*, 8(1), 015023.

Li, H., Harvey, J. T., Holland, T. J., and Kayhanian, M. (2013). “Corrigendum: The use of reflective and permeable pavements as a potential practice for heat island mitigation and stormwater management.” *Environmental Research Letters*, 8(4), 049501.

Liu, K., Wang, Z., Jin, C., Wang, F., and Lu, X. (2015). “An experimental study on thermal conductivity of iron ore sand cement mortar.” *Construction and Building Materials*, 101, 932–941.

Maldonado, O. (1992). “Pulse method for simultaneous measurement of electric thermopower and heat conductivity at low temperatures.” *Cryogenics*, 32(10), 908–912.

Mamlouk, M., and Zaniewski, J. (1998). “Pavement Preventive Maintenance: Description, Effectiveness, and Treatments.” *Flexible Pavement Rehabilitation and Maintenance*.

Meneses, S., and Ferreira, A. (2014). “Flexible pavement maintenance programming considering the minimisation of maintenance and rehabilitation costs and the maximisation of the residual value of pavements.” *International Journal of Pavement Engineering*, 16(7), 571–586.

Miled, K., and Limam, O. (2016). “Effective thermal conductivity of foam concretes: Homogenization schemes vs experimental data and FEM simulations.” *Mechanics Research Communications*, 76, 96–100.

Promentilla, M., Cortez, S., Papel, R., Tablada, B., and Sugiyama, T. (2016). “Evaluation of Microstructure and Transport Properties of Deteriorated Cementitious Materials from Their X-ray Computed Tomography (CT) Images.” *Materials*, 9(5), 388.

Qin, Y. (2015). “A review on the development of cool pavements to mitigate urban heat island effect.” *Renewable and Sustainable Energy Reviews*, 52, 445–459.

Santamouris, M. (2013). “Using cool pavements as a mitigation strategy to fight urban heat island—A review of the actual developments.” *Renewable and Sustainable Energy Reviews*, 26, 224–240.

Scoarnec, V., Hameury, J., and Hay, B. (2014). “A New Guarded Hot Plate Designed for Thermal-Conductivity Measurements at High Temperature.” *International Journal of Thermophysics*, 36(2-3), 540–556.

Tavman, I. (1996). “Effective thermal conductivity of granular porous materials.” *International Communications in Heat and Mass Transfer*, 23(2), 169–176.

Tian, B., Liu, Y., Niu, K., Li, S., Xie, J., and Li, X. (2014). “Reduction of Tire-Pavement Noise by Porous Concrete Pavement.” *Journal of Materials in Civil Engineering*, 26(2), 233–239.

Torres, A., Hu, J., and Ramos, A. (2015). “The effect of the cementitious paste thickness on the performance of pervious concrete.” *Construction and Building Materials*, 95, 850–859.

Tsai, C.-T., Kung, G. T.-C., and Hwang, C.-L. (2010). “Use of high performance concrete on rigid pavement construction for exclusive bus lanes.” *Construction and Building Materials*, 24(5), 732–740.

Ukrainczyk, N., and Matusinović, T. (2010). “Thermal properties of hydrating calcium aluminate cement pastes.” *Cement and Concrete Research*, 40(1), 128–136.

Wang, J., Carson, J. K., North, M. F., and Cleland, D. J. (2006). “A new approach to modelling the effective thermal conductivity of heterogeneous materials.” *International Journal of Heat and Mass Transfer*, 49(17-18), 3075–3083.

Wang, Q., Shi, Y., Shi, J., Zhang, Y., and Liu, W. (2015). “An experimental study on thermal conductivity of ceramsite cellular concrete.” *Proceedings of the 2015 International Conference on Structural, Mechanical and Material Engineering*.

Wong, H., Zimmerman, R., and Buenfeld, N. (2012). “Estimating the permeability of cement pastes and mortars using image analysis and effective medium theory.” *Cement and Concrete Research*, 42(2), 476–483.

Yoon, S., Macphee, D. E., and Imbabi, M. S. (2014). “Estimation of the thermal properties of hardened cement paste on the basis of guarded heat flow meter measurements.” *Thermochimica Acta*, 588, 1–10.

Zawilski, B. M., Littleton, R. T., and Tritt, T. M. (2001). “Description of the parallel thermal conductance technique for the measurement of the thermal conductivity of small diameter samples.” *Review of Scientific Instruments*, 72(3), 1770.

Zhang, M., He, Y., Ye, G., Lange, D. A., and Breugel, K. V. (2012). “Computational investigation on mass diffusivity in Portland cement paste based on X-ray computed microtomography (μCT) image.” *Construction and Building Materials*, 27(1), 472–481.

Zhang, R., Jiang, G., and Liang, J. (2015). “The Albedo of Pervious Cement Concrete Linearly Decreases with Porosity.” *Advances in Materials Science and Engineering*, 2015, 1–5.

Zhao, D., Qian, X., Gu, X., Jajja, S. A., and Yang, R. (2016). “Measurement Techniques for Thermal Conductivity and Interfacial Thermal Conductance of Bulk and Thin Film Materials.” *Journal of Electronic Packaging*, 138(4), 040802.